

Materials characterization of FRP composite seismic retrofits after long-term service in a subarctic Alaskan environment

Sandra Milev^a, David G. Goodwin Jr.^b, Siamak Sattar^b, Jovan Tatar^{a,*}

^a University of Delaware, Department of Civil and Environmental Engineering, Center for Composite Materials, Newark, DE 19716, United States

^b National Institute of Standards and Technology, Engineering Laboratory, Gaithersburg, MD 20899, United States

ARTICLE INFO

Keywords:

FRP
Retrofits
Composites
Chemical degradation
Durability

ABSTRACT

This study assesses physical and chemical properties of fiber reinforced polymer (FRP) composite materials aged in Alaska's subarctic climate. Carbon FRP (CFRP) and glass FRP (GFRP) samples were collected in 2019 from the exterior and interior of Ted Stevens International Airport (TSIA, retrofitted in 2008) and McKinley Tower (MKT, retrofitted in 2004). Differential scanning calorimetry (DSC) was used to measure glass transition temperature (T_g) and physical aging, FTIR and Raman spectroscopy were used to investigate potential chemical degradation and degree of cure, and scanning electron microscopy (SEM) to evaluate cross-sectional microstructure, respectively. The results indicate that exposure to the subarctic climate had minimal effect on the composites' T_g and chemical properties. The variability in fiber content at MKT and thermal properties at TSIA suggest there were likely some inconsistencies in the FRP installation that may affect load-carrying capacity. Furthermore, some microcracks were observed in the FRP retrofits which may have resulted from a combination of poor fiber impregnation and thermal cycling.

1. Introduction

Externally bonded fiber reinforced polymer (FRP) composites are used to extend the service life of deteriorated or structurally deficient reinforced-concrete (RC) structures [1–4]. However, methodology to estimate the service life of FRP retrofits is still not explicitly specified and durability testing is currently based on laboratory-controlled testing or short-term testing under natural weathering conditions (i.e., outdoors) [5]. The durability of FRP is directly related to the following: 1) initial properties of the composite and quality of installation, and 2) environmental exposure such as moisture, freeze–thaw cycles, and UV radiation, which can cause severe physical and chemical aging phenomena.

FRP composites used for structural retrofitting are, in most cases, fabricated using a wet lay-up process. In a wet lay-up process, carbon or glass fabric is impregnated with a thermoset resin (typically a two-component system, such as epoxy, mixed on-site) and bonded to the concrete surface; the thermoset resin then becomes an integral part of the structural system when cured. FRPs can be bonded to the tension face of concrete beams to increase flexural capacity, or to the sides of

beams to increase shear capacity [6]. FRP fabric wraps have also been used for flexural and shear strengthening of columns and for confinement of columns [7]. On the construction site, parameters that affect the epoxy curing reaction include: (1) the curing temperature (T_{cure}) which is a result of the ambient temperature and (2) the proportion of resin to hardener [8]. Controlling curing temperature and humidity on-site is not easy and can adversely affect the long-term performance of FRP retrofits. Data from recent field studies [9] indicate that bond strength after long-term exposure is lower when FRP is installed under relatively cool (12 °C) and hot temperatures (30 °C) compared to a temperature of 24 °C. Due to shorter pot-life and greater degree of cure at a higher temperature, the resin may not completely saturate the fiber fabric, while at lower temperature, prolonged curing can lead to moisture absorption by the resin. Slight variations in the proportion of resin to hardener are also possible. In epoxies, which are the most commonly used type of thermoset resin for FRP retrofits, variations can occur in the molar amine-epoxy ratio r ($r = |A|/|E|$, where $|A|$ and $|E|$ are the number of gram-equivalents of amine and epoxy monomers, respectively). As observed in a study of FRP retrofits applied at several building sites, r can vary from 0.4 to 1.6 [10]. This uncertainty in amine-epoxy ratio

* Corresponding author at: University of Delaware, Department of Civil and Environmental Engineering, Center for Composite Materials, 301 DuPont Hall, Newark, DE 19716, United States.

E-mail address: jtatar@udel.edu (J. Tatar).

<https://doi.org/10.1016/j.conbuildmat.2022.127810>

Received 20 December 2021; Received in revised form 14 April 2022; Accepted 7 May 2022

Available online 19 May 2022

0950-0618/© 2022 Elsevier Ltd. All rights reserved.

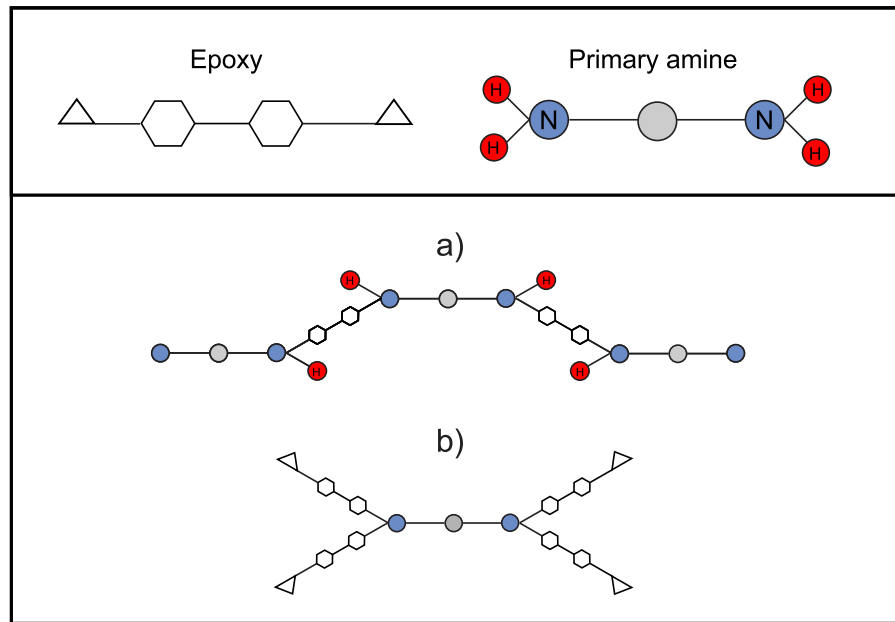


Fig. 1. Curing reactions: a) primary amine addition and b) secondary amine addition.

suggests that FRP retrofits could have variable properties depending on installation procedures.

The glass transition temperature (T_g) of epoxy, or the temperature at which the hardened resin transitions from a glassy state to a rubbery or viscous state, is directly affected by the temperature at which epoxy is cured (T_{cure}) [11]. T_{cure} affects the rate of the two basic curing reactions (Fig. 1) in epoxy: (1) linear polymerization which is a result of a primary-amine reaction with epoxide (a relatively low activation energy and relatively low T_{cure} required), and (2) cross-linking which involves secondary-amine reaction with epoxide (a relatively higher activation energy and higher T_{cure} required for reactant mobility) [12,13]. At lower temperatures (i.e., lower T_{cure}), the cross-linking process terminates before complete conversion of secondary amines is achieved, as curing becomes diffusion controlled and the rate of chemical reaction becomes very low [14,15]. The extent of cross-linking reaction is crucial for obtaining hardened epoxy with high T_g values—it has been experimentally demonstrated that the increase in T_g can be up to 80 % due to cross-linking, compared to 20 % due to linear polymerization [16]. The use of significantly more or less than the stoichiometric amount of curing agent leads to decreased cross-linking density and, thus, lower T_g [17,18]. Possible network structures for different stoichiometric ratios are shown in Fig. 2; branched structures tend to form when non-stoichiometric mixtures ($r > 1$ or $r < 1$) are cured, while cross-linked structures form with stoichiometric mixtures, or when $r = 1$. Reduction of T_g from 87 °C to 63 °C has been reported in mixtures with 20% excess of epoxy, while reduction of T_g from 87 °C to 57 °C has been reported with 50 % excess of amines [19].

According to ACI 440.2R [20], FRP retrofits are suitable for civil engineering applications if their T_g is at least 15 °C greater than the maximum expected service temperature. Exposing partially cured epoxy to a temperature higher than the initial T_{cure} , but lower than the T_g , is a process commonly referred to as the *continuation of curing*, and is desirable in civil engineering applications because it can lead to additional cross-linking and a subsequent increase in T_g [21]. However, exposure to temperatures close to or higher than T_g (hereon referred to as *post-curing*), during the service life of an FRP composite, should be prevented in structural elements to avoid a loss or repeated losses of load-carrying capacity [22]. Although the process of reaching a rubbery state near or above the T_g is reversible when service temperatures decrease, loss of load-carrying capacity at any temperature is a concern.

During their service life, composites are often exposed to harsh conditions. Exposure to moisture, UV radiation, freeze–thaw cycles, and elevated temperatures can lead to physical and chemical degradation of composites over time [23]. Plasticization caused by water absorption lowers the T_g by creating a less rigid state due to filling of the space between polymer chains with water [24–27]. Absorption/desorption cycles can also lead to the formation of microcracks in the resin material [28]. Absorbed water in combination with thermal cycling may induce internal stresses (due to expansion of frozen water at low temperatures) and cause microcracking in the matrix and fiber/matrix interphase [29]. When glassy polymers are exposed to temperatures below T_g for an extended time (months, years), changes in their molecular structure occur due to polymer chains gradually forming more dense, energetically favorable regions that move towards a state of equilibrium. This

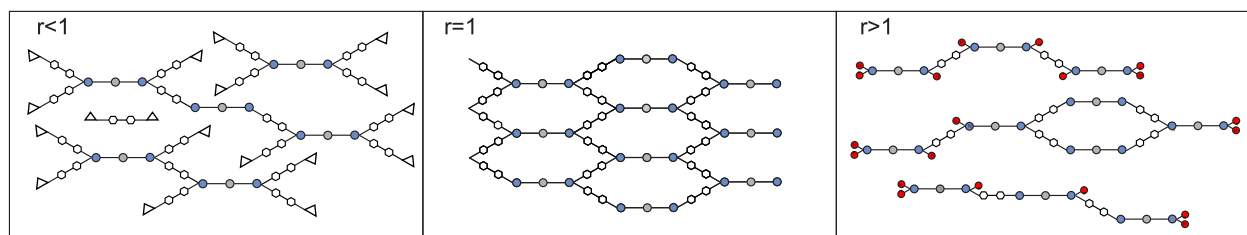


Fig. 2. Possible network structures of the amine-cured epoxy for different mixture formulations: a) excess epoxy ($r < 1$), b) stoichiometric mixture ($r = 1$), and c) excess of amines ($r > 1$).

phenomenon, called *physical aging*, can adversely affect the performance of the FRP retrofit by causing embrittlement and development of internal stresses across the material [30–32]. Physical aging can be quantified by measuring changes in specific enthalpy, which occur due to a reduction in free volume and molecular relaxation [32]. Changes in relaxation enthalpy can be monitored using Differential Scanning Calorimetry (DSC) by measuring the area of the endothermic peak. The area of the endothermic peak increases with molecular relaxation due to the polymer being in a more energetically stable state [30].

Compared to testing mechanical and physical properties, chemical characterization of aged FRP composites is more challenging. One consideration related to chemical characterization is that many scenarios that would lead to chemical change would occur at the composite surface from oxidation, ultraviolet (UV) exposure, and moisture ingress from rain and humidity, while the bulk of the composite would be less affected even under harsh exposure conditions [33–36]. At the concrete substrate surface, chemical degradation of polymer coatings via hydrolysis can be catalyzed by a combination of elevated temperature and the pH (12 to 13) of pore solution in an underlying concrete substrate. In particular, hydrolysis of ester groups can be catalyzed [37]. Epoxy-amines used in FRP application do not typically contain esters and have been shown to not chemically change or lose mass in the presence of concrete (pH of 12.5, 60 °C) [38]. However, unreacted epoxide groups may still hydrolyze in the presence of moisture [38] and elevated temperatures relevant to outdoor conditions. Oxidation is the most common chemical degradation mechanism in epoxy [39–42]. Even though atmospheric oxygen is reactive, oxidation at room temperature is slow [43]. However, oxidation combined with chain scission of epoxy (i.e., photooxidation) can be accelerated by UV radiation [44]. Initial signs of UV-induced damage are gloss loss and surface erosion, which occur as fragmented polymer chains are washed-out from the surface of the polymer. Further UV exposure enables the continuation of the erosion process until fibers are completely exposed [45,46]. In the field, FRP composites are often painted to protect the material from UV exposure and this may mitigate epoxy matrix erosion for some time depending on the efficacy of the paint [47]. Nevertheless, paint loss and chipping can occur during service life. According to the ongoing research on using in-situ monitoring methods, Raman spectroscopy and Fourier Transform Infrared (FTIR) spectroscopy are thought to have good potential as non-destructive methods for monitoring chemical changes of FRP composites in the field [48].

A critical part of the FRP composite system is the bond between the FRP and concrete [27,49,50]. In cold regions, there is a concern that the combination of moisture and cold temperatures can cause bond degradation due to volume expansion of frozen water and thermally-induced stresses due to differential thermal expansion of FRP and concrete [51]. Since our previous study [52] of building retrofits in Alaska, AK revealed some issues with the bond at TSIA and MKT—most probably due to a combination of moisture and freeze–thaw cycles—the effect of cold weather on *bond durability* is not the focus of this paper.

Several studies investigated the durability performance of epoxy materials under freeze–thaw cycles using standardized conditioning procedures or short-term natural weathering [29,51,53–57]. The general lack of data from field studies, which are recognized as the most effective method for assessing the durability of FRP materials, still represents a barrier to accurately predict their usable lifetime. Furthermore, more data on low-temperature curing, which can be adversely affected due to earlier material vitrification [58] and moisture uptake, is needed for wider application of FRP retrofits in cold outdoor environments, such as in Alaska.

This study presents the material characterization of FRP composites aged in a cold climate. Specifically, FRP material samples were collected from Ted Stevens International Airport after 11 years in service, and from McKinley Tower after 13 years in service. This article identifies some of the gaps in field metrology of FRP and provides valuable information on the physical properties of FRP retrofits, with the objective

to serve as a benchmark in future durability studies and development of laboratory and field materials characterization methods, accelerated weathering test methods and well-controlled outdoor weathering studies, design guidelines, and application of FRP as retrofitting method for reinforced concrete structures.

2. Materials and experimental methods

2.1. Materials

Material characterization was conducted on FRP composite samples collected from FRP retrofits installed on two buildings in Anchorage, AK: Ted Stevens International Airport (TSIA) and the McKinley Tower (MKT). In Terminal 2 at TSIA, a total of 35 columns were wrapped with Carbon FRP (CFRP) in 2008. Retrofits at MKT, installed in 2006 (most probably installation started in March 2006 and was completed in May 2006, [59]) included CFRP and glass FRP (GFRP) applied to columns, walls, beams, and slabs. According to the available documentation, the composite system applied at TSIA and MKT was HEX-3R Structural Composite System, composed of unidirectional carbon or glass fiber fabric and ambient-cured, two-component epoxy matrix. According to the manufacturer's data sheets, an application temperature range of 10 °C to 40 °C was suggested. T_g of 51 °C was reported for this epoxy matrix after seven days of curing in a controlled laboratory setting. During their service life, FRP retrofits on the exterior of TSIA and MKT were exposed to extremely harsh environments typical for Anchorage, AK which is located in a subarctic climate zone with monthly highest maximum temperatures in July from 21 °C to 32 °C, monthly lowest minimum temperatures in January from –30 °C to –12 °C, and an average relative humidity of 70 % [60].

GFRP and CFRP material samples, between 20 mm and 50 mm in diameter, were collected in Anchorage, AK in January and September 2019 from the exterior and interior of TSIA and MKT using either a core-saw drill or pull-off test. Twenty-one samples were tested in total (Table 1). Samples from TSIA consisted of two unidirectional FRP plies. GFRP samples collected from the exterior wall of MKT include two unidirectional plies in the horizontal and vertical direction. GFRP samples collected from the interior columns consisted of at least two unidirectional plies. Samples from the north and south wall of MKT were one-ply unidirectional CFRP. An explanation of sample nomenclature is illustrated in Fig. 3. The effect of environmental conditions on thermal

Table 1
Test samples collected at TSIA and MKT.

	Sample name	Material	Experiment
1	TSIA-CF-A-E-1	CFRP	DSC (3), ATR (3), Raman (3)*
2	TSIA-CF-A-E-3 (PT) **	CFRP	TGA (3)
3	TSIA-CF-A-E –6	CFRP	DSC (3), ATR (3), Raman (3), SEM (1)
4	TSIA-CF-B-E-1	CFRP	DSC (3), ATR (3), Raman (5)
5	TSIA-CF-B-E-2	CFRP	DSC (3), ATR (3), Raman (6)
6	TSIA-CF-B-E-3	CFRP	TGA (3)
7	TSIA-CF-C-E-1	CFRP	DSC (3), ATR (3), Raman (5)
8	TSIA-CF-C-E-2	CFRP	DSC (1), ATR (3), Raman (6)
9	TSIA-CF-A-I-1	CFRP	DSC (3), ATR (2), Raman (4)
10	TSIA-CF-A-I-2 (PT)	CFRP	TGA (3)
11	TSIA-CF-B-I-1	CFRP	DSC (3), ATR (3), Raman (5)
12	TSIA-CF-B-I-2	CFRP	DSC (3), ATR (2), Raman (4), SEM (1)
13	MKT-GF-E-E-2	GFRP	DSC (3), ATR (3), Raman (3), SEM, TGA (2)
14	MKT-GF-E-E-3	GFRP	DSC (3), ATR (3), Raman (3)
15	MKT-CF-S-E-1	CFRP	DSC (2), ATR (3), Raman (3), TGA (2)
16	MKT-CF-S-E-2	CFRP	DSC (3), ATR (3), Raman (3), SEM (1)
17	MKT CF-N-E-1	CFRP	TGA (2)
18	MKT-CF-N-E-2	CFRP	DSC (3), ATR (3), Raman (3), SEM (1)
19	MKT-CF-N-E-3	CFRP	DSC (3), Raman (3)
20	MKT-GF-A-I-1	GFRP	DSC (2), ATR (2), Raman (3)
21	MKT-GF-A-I-2 (PT)	GFRP	SEM (1), TGA (3)

*Number in the parenthesis indicates number of tested replicates.

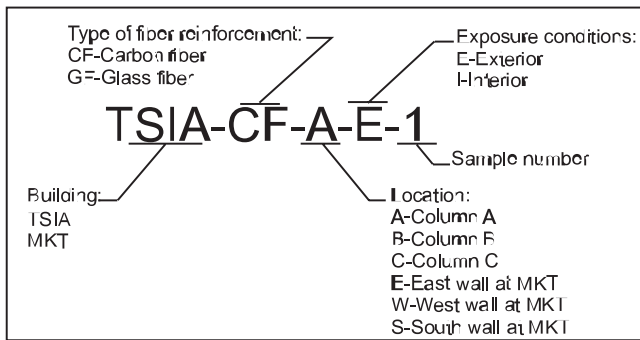


Fig. 3. Sample nomenclature.

properties and chemical changes was investigated by comparing test results of the exterior samples with those of the interior samples when possible.

2.2. Experimental methods

2.2.1. Thermal Analysis—Differential scanning calorimetry and Thermogravimetric analysis

DSC measurements were selected instead of Dynamic Mechanical Analysis (DMA) to determine T_g . DMA is considered to be more sensitive than DSC because it measures dynamic modulus and a damping coefficient, which change considerably when the structure changes from a glassy to a rubbery state [61]. However, DSC was more appropriate for this study than DMA because it required a much smaller sample size and is not dependent on the material's mechanical properties, which may have been modified during sample collection. Considering that the size of the samples collected in Anchorage was between 20 mm and 50 mm in diameter (Fig. 4), DSC was selected as the most appropriate testing method. FRP samples were collected from several columns at TSIA that were accessible. FRP was collected from only one interior column at MKT due to accessibility issues.

DSC experiments were performed using a Netzsch 214 Polyma (Selb, Germany) thermoanalyzer. Sample preparation involved using a 6 mm core-saw drill (Fig. 4) to cut out three circular samples. A relatively small number of replicates were run considering the good repeatability (<1 °C) of DSC measurements. Circular samples were sliced with a razor blade to remove thin layers that were in contact with concrete on one side and to remove the paint on the front side. Sliced replicates, each weighing between 5 mg and 20 mg, were placed into a tared aluminum pan and

weighed using a Mettler Toledo microbalance. To achieve good heat transfer between the pan and the FRP material inside, a mineral oil (Krytox GPL 107 fluorinated synthetic oil, The Chemours Company FC, LLC, Wilmington, DE, US) was used. “Krytox” oil is commonly used to enhance thermal contact between the sample and crucible [62]. Since Krytox oil is chemically inert and stable from temperatures of -95 °C to 340 °C, its presence did not affect the DSC experiment results. The samples were covered with a pierced aluminum lid and sealed with a manual press. Piercing the lid of the crucible was necessary to prevent pressure build-up due to potential evaporation. Each experiment was performed by heating the samples from -20 °C to 250 °C at a heating rate of 10 °C /min under a nitrogen atmosphere. The results are presented as the average and one standard deviation of the DSC measurements taken for three replicates of the same sample.

T_g and enthalpy relaxation were evaluated from DSC curves (Fig. 5). The reported T_g is a midpoint temperature in the glass transition range in the first heat run; it specifically corresponds to the point on the thermal curve that is an arithmetic average between the extrapolated onset of the glass transition (T_o) and the extrapolated end temperature (T_e) of the glass transition [63]. Enthalpy relaxation, as a measure of physical

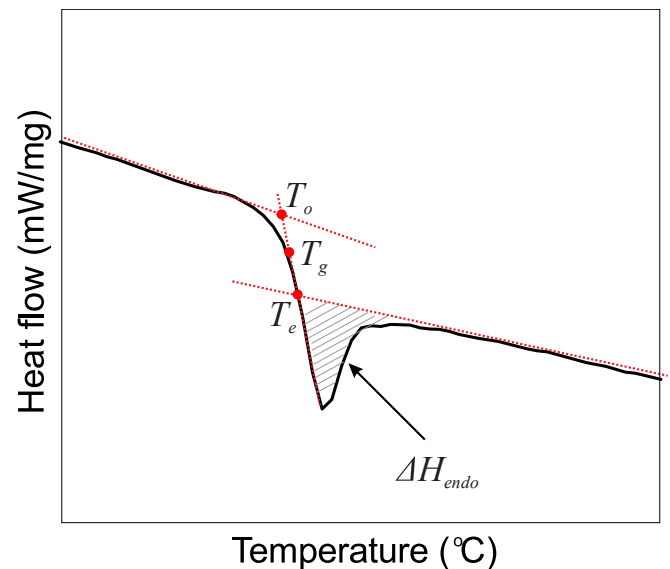


Fig. 5. Example of DSC curve with labels of transitions, endpoints, and enthalpy relaxation peak.

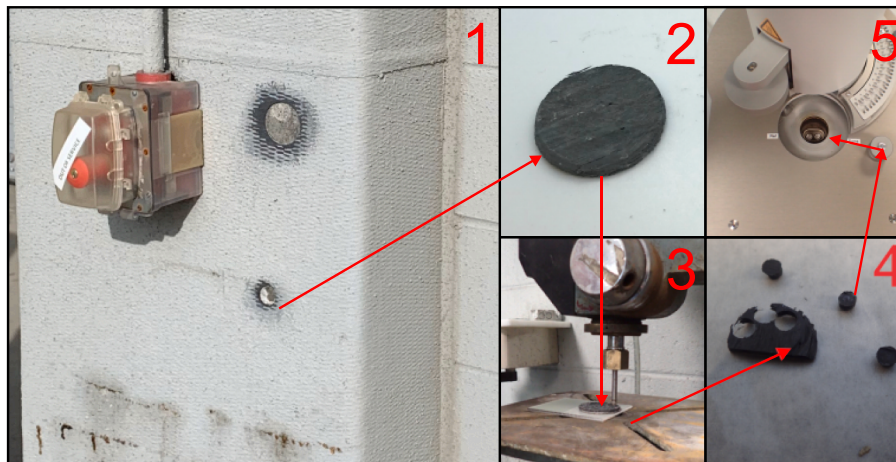


Fig. 4. Sample preparation for DSC: 1) Exterior column at TSIA retrofitted with CFRP 2) 20 mm sample collected from TSIA using core-saw drill 3) and using a 6 mm core-saw drill to extract 4) three circular replicates 5) with specimens ready to be crimped.

aging, was analyzed by calculating the area under the endothermic peak ΔH_{endo} in the glass transition region with an added linear baseline.

Thermogravimetric analysis (TGA) was utilized to measure the weight fraction of carbon and glass fibers in the composite samples. The experiments were conducted on a TA Instruments Q500 Thermogravimetric Analyzer under a nitrogen atmosphere to prevent carbon fiber oxidation. The samples weighed approximately 15 mg (prepared following the same procedure used for DSC experiments) and were heated under nitrogen atmosphere to 600 °C at a rate of 10 °C/min and held isothermal for 80 min. The heating program was selected according to prior research to maximize removal of epoxy matrix while limiting carbon fiber weight loss [64,65]. To assess volume fraction for the TSIA and MKT retrofits, values of 1.77 g/cm³ and 2.55 g/cm³ for carbon and glass fiber densities, respectively, and 1.16 g/cm³ for the density of epoxy were used as specified in materials' data sheets.

2.2.2. Spectroscopy—Fourier-Transform infrared spectroscopy and Raman spectroscopy

Fourier transform (FT)-infrared spectra were recorded on the front (exposed to the environment) surface of FRP composites in attenuated reflection mode (ATR-FTIR) to investigate potential chemical degradation. The front surface was sanded to remove the paint. Sanding was followed by air-blowing with compressed air, without use of solvents to clean the sample surface. The approach for paint removal here was different than for DSC tests, where paint was removed with razor blade. The reason for choosing a different approach is that in the DSC measurements the goal was to measure bulk properties, while FTIR was used for near-surface measurements. Micro-FTIR experiments were carried out on the cross-section of the samples to determine if chemical changes observed in the FTIR spectra extended beyond the surface layer towards the concrete substrate. Spectra were collected using an FTIR spectrometer (Nicolet iS50 FTIR) equipped with an ATR accessory and broad-band DTGS (deuterated triglycine sulfate) detector. A diamond-type Iia crystal and a 45° incident angle were used for all ATR-FTIR measurements. Spectra were collected using 128 scans with a 4 cm⁻¹ resolution. Each background was collected within 100 min of specimen spectrum collection and subtracted from the specimen spectrum. ATR-FTIR spectra were baseline corrected using Origin software. For all spectra, the same number of baseline points and similar wavenumber positions for each baseline point were used during baseline correction (even after normalization, peak widths varied among the spectra of different samples and baseline points had to be adjusted; however, this was not done in the region containing peaks of interest). All spectra were normalized to the 1508 cm⁻¹ band of the interior MKT 50 mm sample, an aromatic stretch that was consistently present across all spectra and is unlikely to be affected by environmental degradation [36]. The 1508 cm⁻¹ band was only used in CFRP samples when carbon fibers were not exposed due to erosion or poor saturation, as the benzene rings within carbon fibers can contribute to this band. The lack of fibers in the spectra was confirmed by the absence of increased background signal across the spectra related to infrared absorption of the black fibers. At least three replicate areas were measured for each specimen and the replicate spectra were averaged after baseline correction. ATR-FTIR spectra are presented in terms of absorbance. Micro-FTIR experiments were performed on a Nicolet iN10 MX infrared microscope with an ATR attachment (4 cm⁻¹, 64 scans) with a germanium crystal. The aperture size was 100 × 100 μm. At least two replicate areas were measured for each specimen and five replicate measurements for each area. These spectra were not baseline corrected or normalized; they were used only to determine if the same peaks are present in the spectra collected on the cross section and spectra of the sample surface.

Raman spectra were recorded with a Senterra II Raman Microscope (Bruker Optics, Inc.), a 785 nm laser, and automatic wavenumber calibration using a built-in HeNe reference. The laser beam was focused on the FRP sample cross-section using a 50x microscope objective. The samples were analyzed with a power of 10 mW for CFRP and 25 mW for

GFRP, conditions that were found to maximize signal while minimizing background fluorescence. Spectra consisted of 5 co-additions and 10 s integration time (scans were recorded at 4 cm⁻¹ resolution from 400 cm⁻¹ to 4000 cm⁻¹). Baseline correction was performed in OPUS 8.2.28 software, using a concave rubberband correction (20 iterations, 1000 points). For each specimen, at least three baseline-corrected spectra were averaged. For comparison, all spectra were normalized to the 1609 cm⁻¹ band of TSIA-CF-A-E-6 sample. The band at 1609 cm⁻¹ corresponds to an aromatic ring stretch [66] and is not expected to change during chemical degradation.

2.2.3. Microstructure Characterization—Scanning electron microscopy

SEM images were collected for six samples (Table 1) to investigate potential degradation of the resin matrix, fibers, and their interface. For the microscopic analysis, pieces of FRP were cut using a water-cooled diamond saw and impregnated in epoxy. These samples were sequentially sanded with different grits (from 120 to 2400 grits size) and subsequently polished with an alumina powder slurry to obtain a smooth surface. Samples were coated for 20 s with a layer of gold/palladium in a Denton Vacuum sputter coater to minimize charging of the samples under the electron beam. Images were recorded on a Hitachi TM3030 tabletop microscope in secondary electron (SE) mode using coated and uncoated samples. Different accelerating voltages, 5 kV or 15 kV, were used to obtain optimal conditions for imaging.

3. Results and discussion

3.1. Glass transition temperature, degree of cure, and physical aging

Fig. 6 shows a comparison of T_g values obtained for all tested exterior and interior retrofits from TSIA and MKT. The observed T_g values on the exterior CFRP retrofits at TSIA were between 57 °C and 74 °C. Interior samples at TSIA had T_g values that also spread over a wide range, varying from 52 °C to 62 °C. T_g values for exterior retrofits at TSIA were generally higher than T_g values of interior retrofits. Generally, lower T_g values for the interior columns were observed which was likely due to reduced post-curing under ambient conditions. In contrast, exterior FRP retrofits generally had higher T_g values, indicating that post-curing likely occurred during hot summer weather. A possible reason for the significant variation in exterior T_g data may be exposure to lower T_{cure} at the time of FRP installation at different airport locations, which could have caused early termination of the curing process and resulted in a less cross-linked polymer network and lower T_g . The presence of moisture outdoors, especially at low cure temperatures where curing takes longer, might have also led to plasticization; this would have increased the free volume in the cross-linked network and decreased the T_g values as a result. Variations in epoxy batch mix proportions may also have played a role. However, variations observed among different samples from the same column (e.g., exterior column A) cannot be attributed to differences in environmental conditions during installation, because FRP for a specific column was most likely installed all at once. Since DSC sample size is very small, it may be unrepresentative of the bulk material, especially if the epoxy is heterogeneous as a result of inconsistent mixing. The significantly lower T_g value observed in exterior sample TSIA-CF-A-E-1, $T_g=57$ °C, compared to 68 °C measured on another sample (TSIA-CF-A-E-6) from the same column, might have been due to heterogeneity of the epoxy used on that part of the column. The low values of T_g observed for the one interior Column A (TSIA-CF-A-I-1) might also be related to variations in mixture stoichiometry between different locations at TSIA. Low curing temperature and the presence of moisture are also possibilities but were not likely for interior columns in a climate-controlled facility.

At MKT, the T_g value for most exterior and interior samples was approximately 55 °C, except for the CFRP samples collected on the exterior north wall, which had T_g values of 45 °C and 50 °C from two

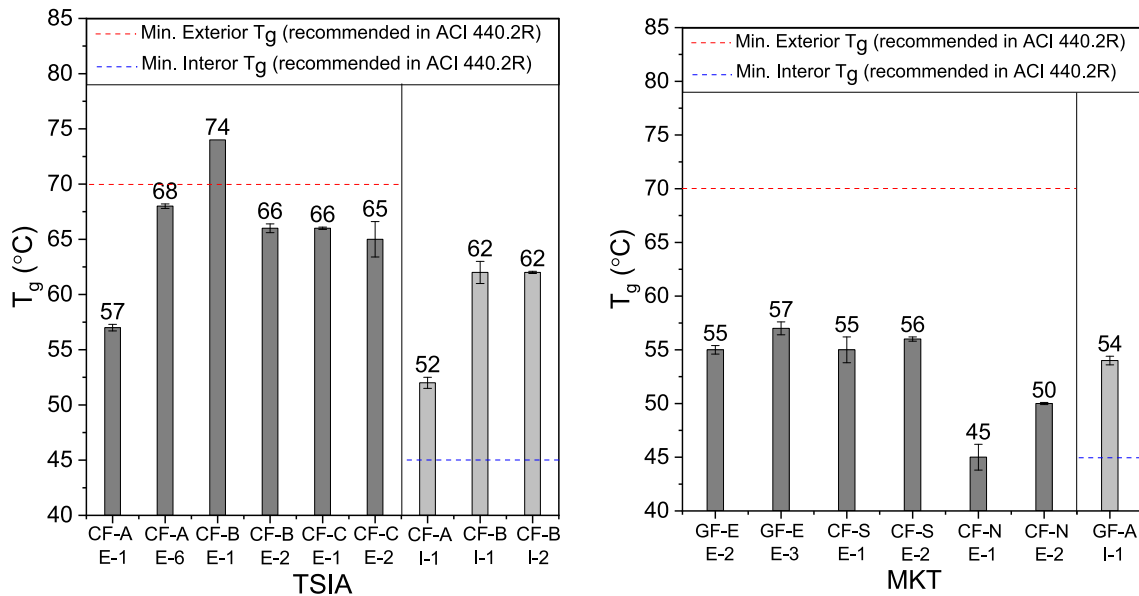


Fig. 6. The average T_g values of FRP specimens collected at MKT and TSIA.

different sample locations (Fig. 6). Again, this can be due to variability in installation on the exterior of MKT (different curing temperatures, variability in the stoichiometry of the epoxy resin and hardener) or the presence of moisture outdoors. Since the interior T_g value was similar to most of the exterior T_g values, there might not have been as much moisture present outdoors during installation, the temperature outside might not have been as low as it was at the airport, or the mix proportions were identical indoors and outdoors.

All samples from MKT had T_g values lower (or equal) than values measured at TSIA, with the exception of TSIA-CF-A-I-1. These results may be different from those of TSIA due to differences in curing temperature or different mix proportioning. Additionally, the chemical structure of the epoxy resin and the type of hardener might have been slightly different between the two buildings, resulting in a different network structure of the hardened epoxy.

T_g is important both as an indicator of mechanical properties of FRP and as a parameter on which maximum service temperature is estab-

lished. According to ACI 440.2R-17, for a dry environment, it is generally recommended that the service temperature of an FRP system not exceed ($T_g - 15\text{ }^\circ\text{C}$) because exposure to elevated temperatures (near T_g) leads to a decrease in stiffness and strength of the polymer matrix. When assessing the adequacy of achieved T_g for FRP retrofits on structures, engineers and end users need to be aware of parameters that can affect measured values. First, depending on the type of technique used (DSC and DMA) and testing parameters, T_g values can vary by $>15\text{ }^\circ\text{C}$ [67,68]. Specimen age and heating rate are other factors that influence T_g and are usually not reported in technical data sheets [69]. Furthermore, a specified concrete surface temperature in different climatic areas is not provided in ACI 440.2R, leaving it to the licensed engineer to specify the expected concrete service temperature. AASHTO requires that T_g is at least $22\text{ }^\circ\text{C}$ higher than the maximum design temperature (defined in AASHTO Bridge Design Specifications [70]). Some guidelines (Bulletin FIB 14, [71]) use maximum shade air temperature in establishing acceptable T_g , which may yield a temperature threshold

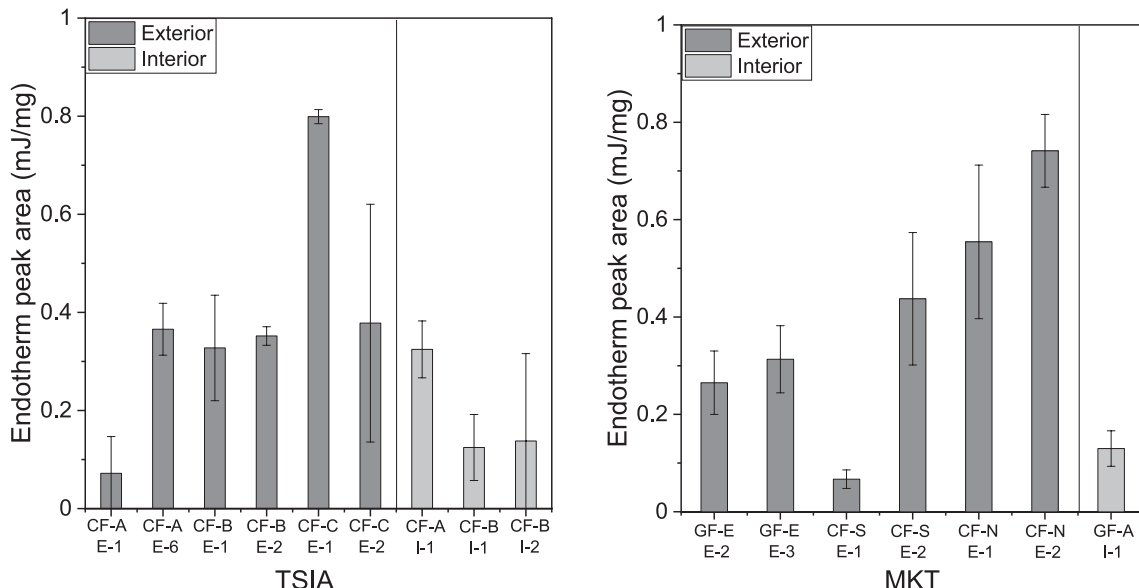


Fig. 7. Typical DSC curves of exterior and interior retrofits at TSIA and MKT.

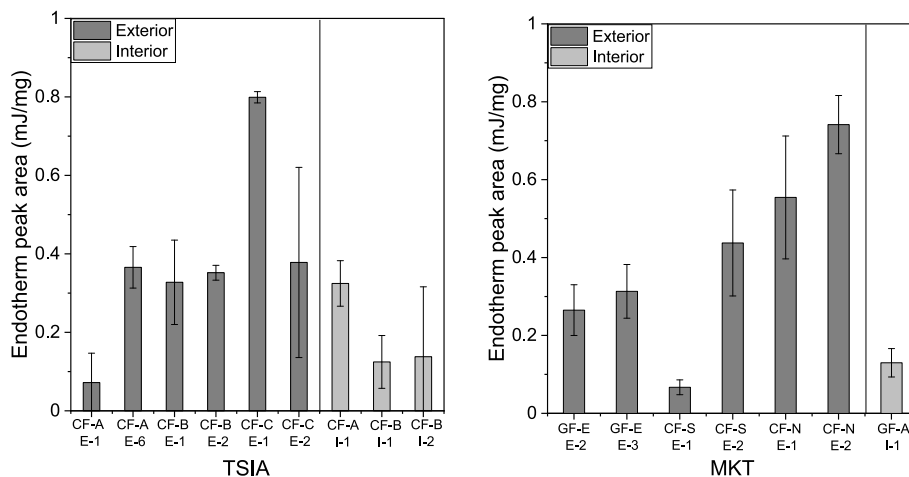


Fig. 8. Comparison of endotherm peak areas ΔH_{endo} .

underestimation in situations when a concrete surface is directly exposed to sunlight. For example, in a study performed in Switzerland, the measured surface temperature on a concrete bridge directly exposed to sunlight was 55 °C, while the air temperature was 33 °C [69].

To evaluate the adequacy of retrofits at MKT and TSIA regarding T_g , measured T_g values were compared with the minimum T_g values recommended in the ACI.440.2R design guideline (Fig. 6). ACI.440.2R recommends that the minimum T_g is at least 15 °C higher than the maximum service temperature. An exterior service temperature of 55 °C was defined according to: 1) suggestions in the literature described above [69] which showed that a concrete surface exposed to direct sunlight temperature was 55 °C, while the air temperature was 33 °C and 2) climate data that shows variation between 21 °C and 32 °C of maximum ambient temperatures in July over the last 15 years in Anchorage, [60]. Interior service temperature was conservatively assumed to be 30 °C. As shown in Fig. 6, measured T_g values for exterior retrofits were lower than the recommended minimum (55 °C + 15 °C) in ACI 440.2R. In contrast, the T_g values for interior retrofits exceeded the minimum needed to maintain optimal mechanical properties.

In Fig. 7, DSC curves show the endothermic peak ΔH_{endo} within the glass transition region. In general, the enthalpy relaxation area increases with more molecular relaxation due to the polymer being in a more energetically stable state [30]. At both buildings, variation of ΔH_{endo} among the samples was observed without obvious trends in the behavior between CFRP and GFRP, or exterior and interior retrofits (Fig. 8). Based on the limited data on interior samples at MKT (only MKT-GF-A-I-1) and exterior samples at TSIA, it appears that the enthalpy relaxation was greater (i.e., integrated area) in exterior retrofits than the interior. Additionally, the greatest enthalpy relaxation was measured on the samples from the north wall of MKT (MKT-CF-N-E-1 and MKT-CF-N-E-2), which had the lowest T_g values. During their service life, specimens were subjected to environmental factors such as moisture, UV light, and thermal cycles, which might have altered the polymers' microstructure. Some researchers have already made attempts to correlate polymer structure with relaxation kinetics [19] and reported that the enthalpy relaxation area increases as degree of cross-linking decreases. Higher molecular relaxation is expected in less cured epoxy resin due to lower cross-linking density and more free volume than a more cross-linked network, which inhibits chain motions. Considering that enthalpy relaxation does not only depend on the degree of cure and mixing ratio of the epoxy resin and hardener, but is also affected by the thermal history and the bond between the matrix and fiber sizing [72], it is difficult to identify reasons for observed variability in the samples from TSIA and MKT without adequate baseline data.

To further investigate differences in the degree of cure between

exterior and interior samples, Raman spectroscopy was used to estimate the concentration of epoxy groups. The band around 1250 cm^{-1} in Raman spectra is commonly used to monitor the consumption of epoxide groups during curing [66,73–75]. The epoxide band at approximately 1250 cm^{-1} overlaps with another band at 1225 cm^{-1} . Peak deconvolution was conducted by fitting Gaussian functions to experimental spectra [76]. Based on the analysis, it was concluded that contribution of 1225 cm^{-1} peak to the maximum intensity of 1252 cm^{-1} is only 3 % (calculated from $I(1225_{@1252})/I(1252)$, Fig. 9), thus interference between 1252 cm^{-1} and 1225 cm^{-1} bands is insignificant (Fig. 9).

The degree of epoxide group conversion was evaluated by dividing the epoxide peak intensity by the band intensity of 1608 cm^{-1} for benzene that was not likely to change with weathering. A greater degree of epoxide group conversion occurred when less epoxide groups were present, which was apparent when there was a lower epoxide band intensity relative to the reference band intensity. The normalized epoxide band intensity H_{1252}^{nor} is calculated as the 1252 cm^{-1} band intensity (H_{1252}) multiplied by the ratio of benzene reference band intensity

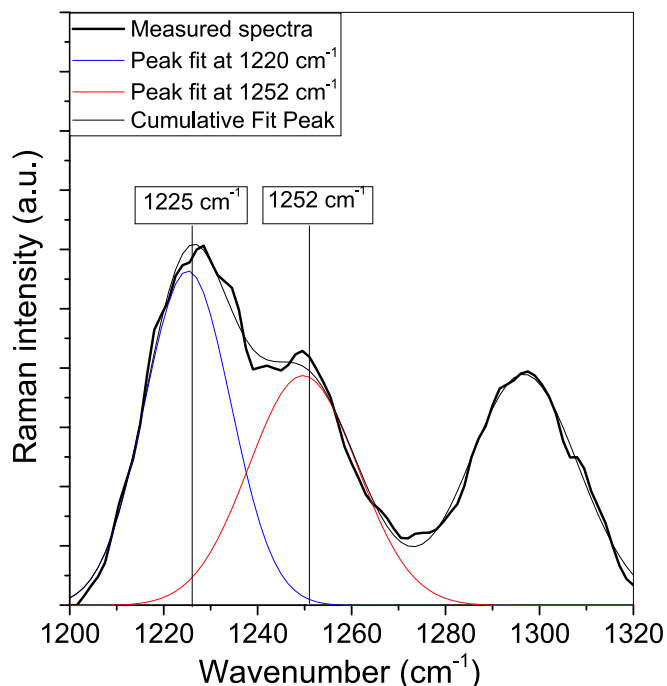


Fig. 9. Deconvolution of Raman bands at 1225 cm^{-1} and 1252 cm^{-1} .

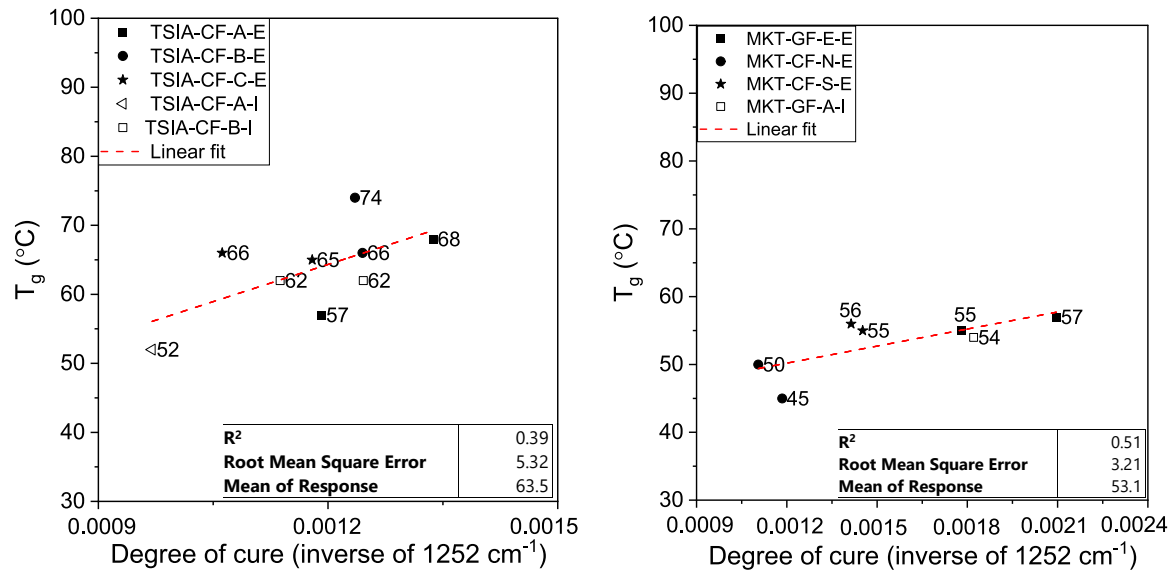


Fig. 10. Correlation between the degree of cure (inverse of 1252 cm^{-1}) determined by Raman (epoxide band intensities at 1252 cm^{-1} normalized to the 1608 cm^{-1} benzene reference band intensity of a control sample) and corresponding T_g values at exterior and interior of TSIA and MKT.

(H_{1608}) of the observed sample to the 1608 cm^{-1} benzene reference band intensity of the control sample (TSIA-A-E-6) H_{1608}^{ref} , $H_{1252}^{nor} = H_{1252} \frac{H_{1608}}{H_{1608}^{ref}}$. Inverse values of normalized epoxide band intensities are plotted (Fig. 10) to emphasize the correlation between degree of cure and T_g values.

Data were statistically analyzed to determine if there was a correlation between T_g and epoxy group concentration (Fig. 10) using Pearson's coefficient, r . Pearson's coefficient for the two variables had a value of 0.62 at TSIA and 0.72 at MKT. Statistical analysis (t -test for the slope estimate) showed that the relationship is not statistically significant at 0.05 level ($p = 0.07$, Fig. 10). As shown in many studies [77], T_g is a function of conversion—higher degree of cure (i.e., less unreacted epoxides in the system) results in higher T_g values. However, variation in T_g does not depend only on the degree of cure, it is also a function of the stiffness of the crosslinked chain and the free volume in the network

[16,78]. For the same degree of cure, the presence of moisture or a non-stoichiometric ratio of reacted amine and epoxides, can increase the free volume and lower the T_g [24,79]. Water molecules can infiltrate in between the polymer chains, increasing the free volume and leading to plasticization effects, which decrease T_g [80]. Although pre-cured mixtures with an excess of epoxy groups can lower the T_g significantly, excess of amines can also lower the T_g [19]. A lack of data about the initial ratio of epoxy to amine groups and concentration of amines present in the aged samples, makes it difficult to draw firm conclusions about the degree of cure.

3.2. Spectroscopic characterization of composite matrix

ATR-FTIR data was used to investigate the potential chemical degradation of FRP retrofits. Fig. 11 shows a comparison of the ATR-FTIR spectra of exterior and interior samples from TSIA and MKT. All

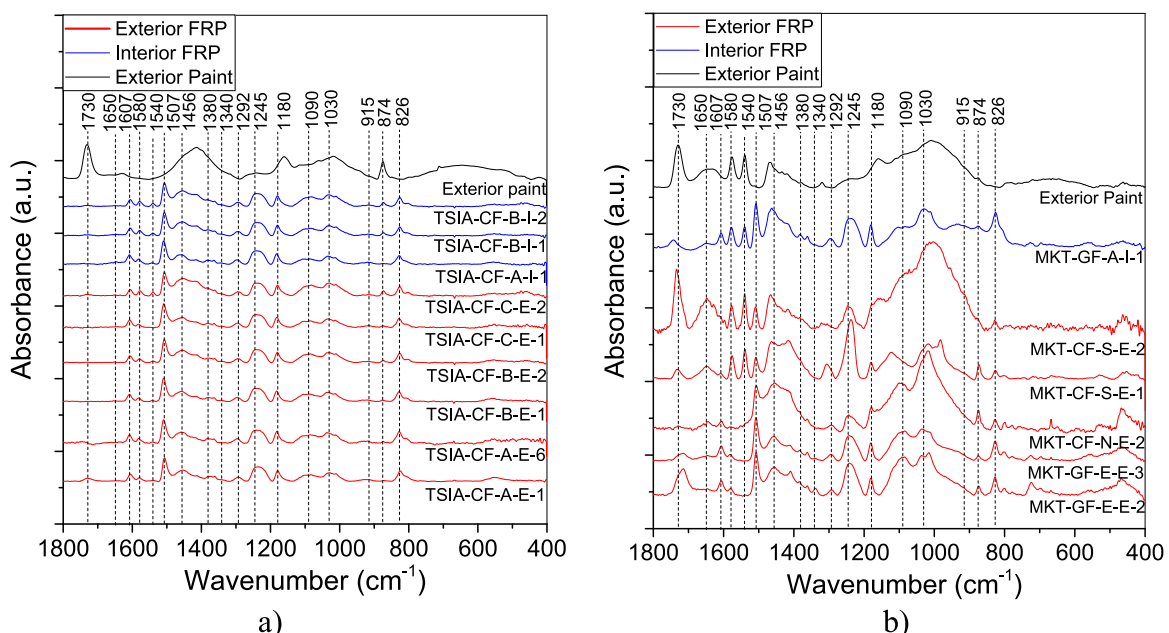


Fig. 11. Comparison of ATR-FTIR spectra from exterior and interior of: a) TSIA and b) MKT.

Table 2
FTIR band assignment.

FTIR Band (cm ⁻¹)	Reference Band(s) (cm ⁻¹)	Assignment
826	831 [86], 824 [39], 827 [87]	Stretching of C-O-C epoxide[86], p-phenylene groups[39], bending of C-H in benzene [87]
874	870 [88]	Carbonate[88]
915	916 [86,89]	Epoxy [86,89]
1030	1036 [86,89,90], 1035 [91]	Substituted aromatic [89], ether [86,90]
1090	1100 [91]	Ether [91]
1180	1184 [89], 1183 [90]	CH ₃ [89], isopropylidene [90]
1245	1232 [86], 1250 [91], 1244 [87]	Ether [87,91]
1292	1293 [39,92]	Twisting of -CH ₂ - [39,92]
1362	1366 [93]	-CH ₃ [93]
1340*	N/A	N/A
1456	1455 [36], 1460 [93]	-CH ₂ [36,93]
1509	1509 [16,42,45]	C-C of benzene ring [16,42,45]
1540*	N/A	N/A
1580	1581-1590 [90], 1584 [93]	Stretching C-H of aromatic ring [90,93]
1607	1610 [91,93]	C = C of benzene ring [91,93]
1650*	N/A	N/A
1726	1732 [87], 1710 [91]	Carbonyl [91]

*Peaks observed in the spectra of field samples, but not assigned to any functional groups since they were not found in the referenced articles.

identified peaks were compared against reference peaks from the literature (see Table 2). In the literature, the peak around 1730 cm⁻¹ has been observed in the spectra of epoxy exposed to UV radiation [21,81,82]. The appearance of a band around 1660 cm⁻¹ is characteristic of an amine-related aging mechanism [35]. The presence of this band was reported in the literature for amine-cured epoxies after thermal aging [83,84], hygrothermal cycling [39], UV exposure [34,81,82], and outdoor weathering [34,85].

For the samples from TSIA, minimal differences between spectra suggest that environmental exposure did not lead to chemical degradation (Fig. 11). However, differences among the spectra on MKT samples were observed at wavenumbers in the range from (1500 to 1750) cm⁻¹—specifically, peaks at 1540 cm⁻¹, 1650 cm⁻¹, and 1730 cm⁻¹ were present in some spectra, but not in others. In addition to the bands observed in the (1500 to 1750) cm⁻¹ region, a variation in the peak intensity at 1245 cm⁻¹, corresponding to the aromatic ether bond, [40,87] was also observed in some spectra. This peak is considered suitable for analysis due to its strong intensity and because it does not overlap with adjacent peaks, unlike other bands in the region from (800 to 1500) cm⁻¹. Peak intensities at 1245 cm⁻¹ were reasonably uniform

among the CFRP retrofits from TSIA, and GFRP retrofits from MKT, which suggests there was no degradation (Fig. 12). On the other hand, notable variation was present between CFRP samples collected from the south and north wall at MKT (Fig. 12). A decrease of the 1245 cm⁻¹ peak, has been reported in the literature as a sign of chain scission of aromatic ethers in amine-cured epoxies exposed to UV radiation [82], hygrothermal aging [39], thermal aging [94].

Inter-crosslink chain scission results in fragmentation of polymer chains and leaching of detached segments [92], which increases free volume in the polymer network and, consequently, decreases *T_g*. To determine if there is a correlation between the 1245 cm⁻¹ peak intensity and the *T_g* values, data were statistically analyzed using linear regression and *t*-test to determine if the slope is significantly different than 0. Fig. 13 shows that there is no correlation between the two variables. This suggests that even if some chain scission had occurred at the ether group (as indicated by a reduction in the 1245 cm⁻¹ peak intensity), it did not significantly affect the cross-linking density in the FRP retrofits.

Investigation of chemical degradation of FRP composites collected in the field using FTIR spectroscopy was challenging for several reasons:

- Before collecting spectra on the front side of all specimens, paint was removed by sanding; however, the intensity of some peaks of interest, such as 1540 cm⁻¹, 1650 cm⁻¹, and 1730 cm⁻¹, might have been obscured due to interference with peaks from remaining paint residue that was not visually apparent (Fig. 11). Although 1540 cm⁻¹, 1650 cm⁻¹ and 1730 cm⁻¹ bands are present in the spectra from MKT, degradation cannot be confirmed because these peaks are also present in the paint spectra (Fig. 11). Additional polishing of the sample surfaces and repeating the measurement showed a decrease in the band height or absence of these bands.
- The literature review showed contradictory peak assignments in different studies. For example, in some studies, the peak at 831 cm⁻¹ is assigned to C-O-C stretching of the epoxide group [93], but in other studies [42,94,95] the same band is related to the C-H vibration of the aromatic benzene group. Decoupling the two peak assignments is difficult and makes this peak unreliable to monitor degradation. Vibrations at 1292 cm⁻¹ are generally assigned to CH₂ [39,92], but it is not clear if the peak corresponds to the backbone twisting/wagging of all -CH₂ groups or, specifically, to -CH₂ in the epoxide ring. Furthermore, the peak at 1340 cm⁻¹ could not be assigned to any functional group after reviewing published literature.
- The selection of a normalization peak is essential for the comparison of peak intensities between spectra collected on different samples. For reliable analysis, it is necessary to normalize all spectra to a band that is not susceptible to degradation under considered environmental conditions. Bands at 1509 cm⁻¹ and 1610 cm⁻¹

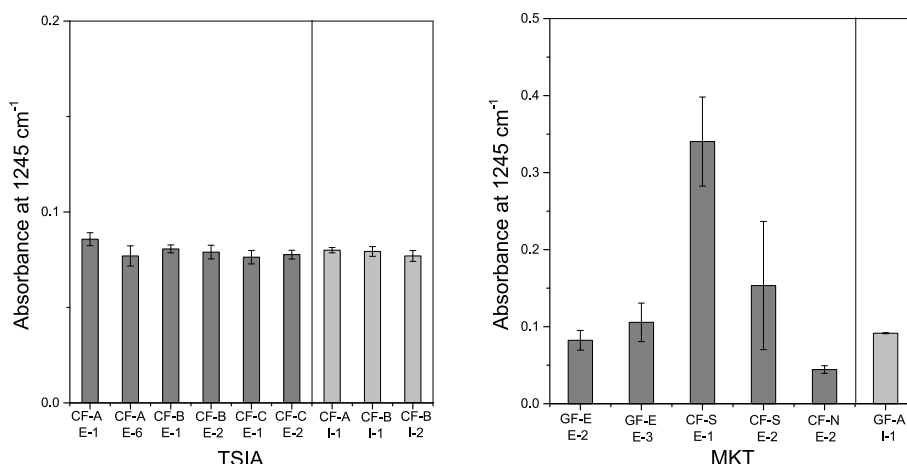


Fig. 12. Comparison of 1245 cm⁻¹ band intensity in FTIR spectra (values normalized to 1510 cm⁻¹) at the exterior and interior of TSIA and MKT.

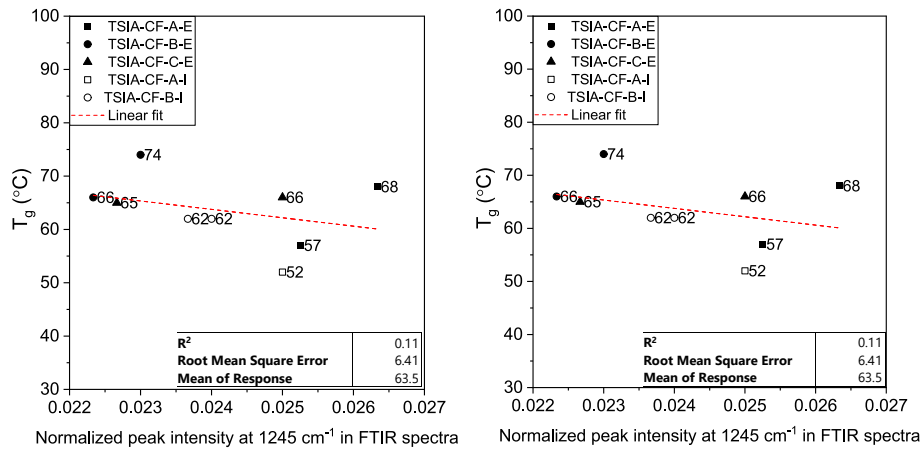


Fig. 13. Peak intensities at 1245 cm^{-1} in FTIR spectra and corresponding T_g values of exterior and interior FRP samples from TSIA and MKT (black symbols represent exterior samples, white symbols represent interior samples).

corresponding to vibrations of C–C and C = C bonds of the aromatic ring, respectively, are commonly used as normalization bands [36,41,93], due to high chemical stability of these bonds within the epoxy network. This band becomes unreliable when carbon fibers become exposed due to epoxy erosion or insufficient saturation, since the benzene rings within carbon fibers can affect this band.

Initially, analyzing spectra collected on the front surface of the FRP was identified as the best approach to evaluate possible degradation since this side was exposed to the environment. However, due to challenges related to the paint sanding (which can disturb the potentially degraded surface), FTIR analysis on the cross-section using micro-FTIR was performed and is considered a helpful solution for the analysis of painted field samples. Micro-FTIR on the sample cross-section near the exposed surface did not show evidence of oxidation by UV exposure as indicated by the absence of the peak in the 1730 cm^{-1} region (Fig. 14). Based on micro-FTIR spectra, if any degradation occurred, it was limited

to the surface layer of $<100\text{ }\mu\text{m}$, smaller than the workable micro-FTIR spot size ($100\text{ }\mu\text{m} \times 100\text{ }\mu\text{m}$).

Raman spectroscopy was used as a complementary tool to ATR-FTIR spectroscopy to provide additional evidence of chemical changes, if any, that occurred in the polymer matrix. Fig. 15 illustrates spectra recorded on the cross-section of the interior and exterior of the epoxy matrix in FRP retrofits from TSIA and MKT. Band assignments, based on previous Raman studies of epoxy resins [66,73,75,96], are shown in Table 3. All identified bands in Table 3 correspond to either epoxide or aromatic group vibrations. It was assumed that the 1610 cm^{-1} band associated with aromatic benzene ring vibration has the lowest probability of changing over time and was used as a reference for normalization. All spectra of interior samples shown in Fig. 15 look similar to the spectra of exterior samples, indicating that the chemical structure of the matrix in the exterior retrofits did not undergo significant chemical changes after being exposed to the outdoor environment in Alaska.

3.3. Thermogravimetric analysis

The fiber weight fraction of eight samples from TSIA and MKT are listed in Table 4. At TSIA, the average fiber weight fractions varied between 46 % and 55 % for the three types of samples. For the four types of MKT samples, average values between 52 % and 71 % were measured. Variability between the replicates of one type (i.e., location) of FRP sample indicates a non-uniform distribution of the fibers, which can be observed in the SEM images (in Section 3.4). More significant variability was noticed between the different locations at MKT. During the field visit at MKT, visual inspection of CFRP retrofits revealed insufficient epoxy saturation of the carbon fabric on the south and north side of MKT. Observed epoxy saturation issues can indicate a potential incompatibility between fiber sizing and epoxy resin or a flawed installation procedure.

Specifications for carbon and glass FRP materials do not define fiber volume fraction limits. Specifying a lower limit of 50 % fiber content (v/v) for unidirectional composites has been suggested by some researchers [98]. ACI 440.1R defines a lower limit on the fiber volume fraction of 50 % for FRP bars. The upper limit has not been established in design guidelines, but it should be noted that for volume fractions higher than (60 to 70) %, composite strength starts to decrease due to the lack of resin holding fibers together [99]. Based on the data shown in Fig. 16, fiber volume fraction was lower than 50% in almost all samples, which is considered to be significantly below the minimum value for unidirectional composites [98]. It is not clear how fiber volume content affects the durability of composites. According to some researchers, CFRP composites with low fiber volume content are more sensitive to moisture uptake, which accelerates the deterioration of the resin and fiber–matrix

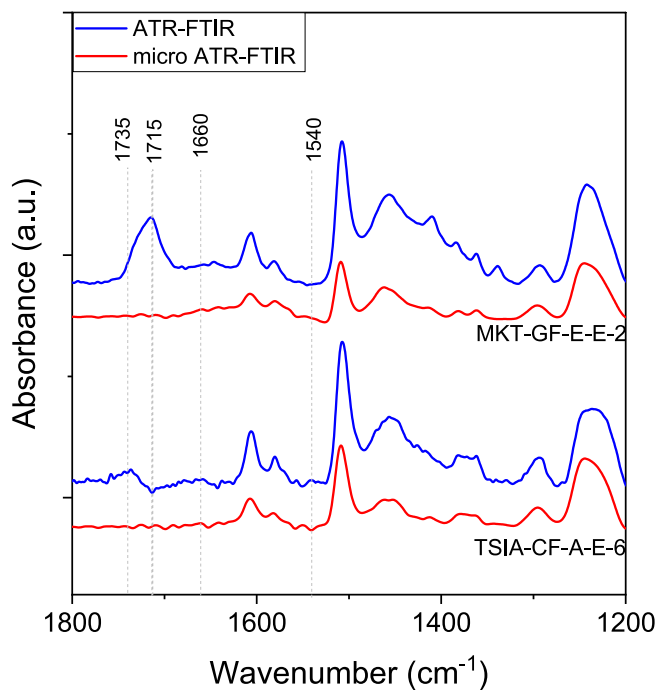


Fig. 14. Comparison of FTIR spectra collected on the cross-section and the surface of FRP samples.

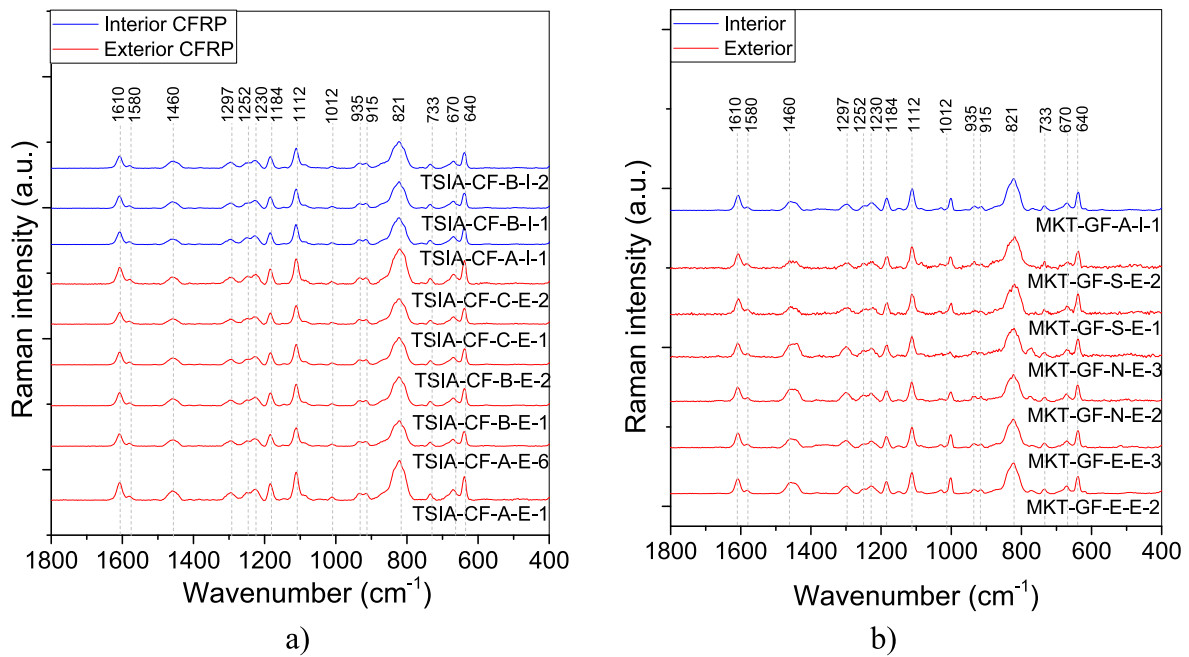


Fig. 15. Comparison of Raman spectra from the exterior and interior of: a) TSIA, b) MKT (only GFRP).

Table 3
Raman peak assignment.

Raman Band (cm ⁻¹)	Reference Band(s) (cm ⁻¹)	Assignment
640	641 [89], 642 [66]	p-sub benzene ring [89], epoxy ring deformation [66]
670	667 [89]	Aromatic C-H out of plane def. [89]
733	736 [66,89]	C-C skeletal [89], epoxy ring deformation [66]
821	819 [89]	Substituted aromatic [89], CH-wag [66]
915	908 [89], 916 [66,74]	epoxy ring deformation [89]
935	936 [66]	CH-wag [66]
1012	1012 [66]	aromatic ring stretch [66]
1112	1113 [89], 1112 [66,97]	Aromatic C-H stretch [89], epoxy ring [66], C-C stretch [97]
1184	1186 [89], 1188 [66]	CH ₃ / <i>gem</i> -dimethyl der. and C-C [66] stretch [89], CH-wag [66]
1230	1232 [89]	C-O stretch [89]
1252	1260 [74], 1252 [66], 1255 [97]	epoxy ring [89]
1297*	N/A	N/A
1460	1470 [89], 1460 [66]	CH ₂ deformation [89]
1580	1580 [66], 1590 [74]	aromatic ring stretch [66]
1610	1610 [66], 1609 [97]	aromatic ring stretch [66]

*Peak observed in the spectra of field samples, but not assigned to any functional groups since it was not found in the referenced articles.

interface [100]. However, others report that composites with higher fiber volume fraction absorb more water than FRP with lower fiber volume fraction. High fiber content may prevent the matrix from fully bonding with the fiber and as a result, microcracks can appear at the fiber/matrix interface and accelerate water diffusion into the composite, thus facilitating the degradation [101,102].

Table 4
Fiber weight fraction determined by TGA.

Specimen	Fiber weight fraction (%)				
	Replicate 1	Replicate 2	Replicate 3	Average	CoV (%)
MKT-GF-E-E	56	49	52	53	6.6
MKT-CF-S-E	56	61	57	58	4.6
MKT-CF-N-E	70	73	70	71	2.4
MKT-GF-A-I	56	46	54	52	10.2
TSIA-CF-A-E	50	42	45	46	8.8
TSIA-CF-B-E	58	48	59	55	11.1
TSIA-CF-A-I	53	53	56	54	3.2

3.4. Microstructure

Fig. 17 shows cross-sectional SEM images of representative exterior and interior CFRP retrofits from TSIA. From low magnification images (Fig. 17a, Fig. 17c), the matrix's non-uniform distribution of kidney-shaped fibers was noted. Compared to commonly used circular carbon fibers, kidney-shaped fibers are used to provide improved interfacial strength due to the increased surface area of the fiber and the interlocking effect enabled by the fiber shape [103]. As observed in high magnification images, there are air voids present, but no signs of fiber degradation, fiber/matrix debonding, or matrix microcracking for the samples from TSIA (Fig. 17b and Fig. 17d). Overall, no difference between exterior and interior retrofits was observed.

CFRP and GFRP samples from MKT had air-voids (Fig. 18a,b,c,f,h), misaligned fibers (Fig. 18c), and non-uniformly distributed fibers (Fig. 18a,c). GFRP did not exhibit defects at the fiber/matrix interface (Fig. 18 b,d); however, cracking in the region with closely-spaced fibers was evident in CFRP (Fig. 18e). This is probably due to poor saturation of the carbon fibers, which was apparent during the field inspection [52] and from TGA analysis (Fig. 16). The interface between the fiber and matrix is the most probable location for crack initiation due to its

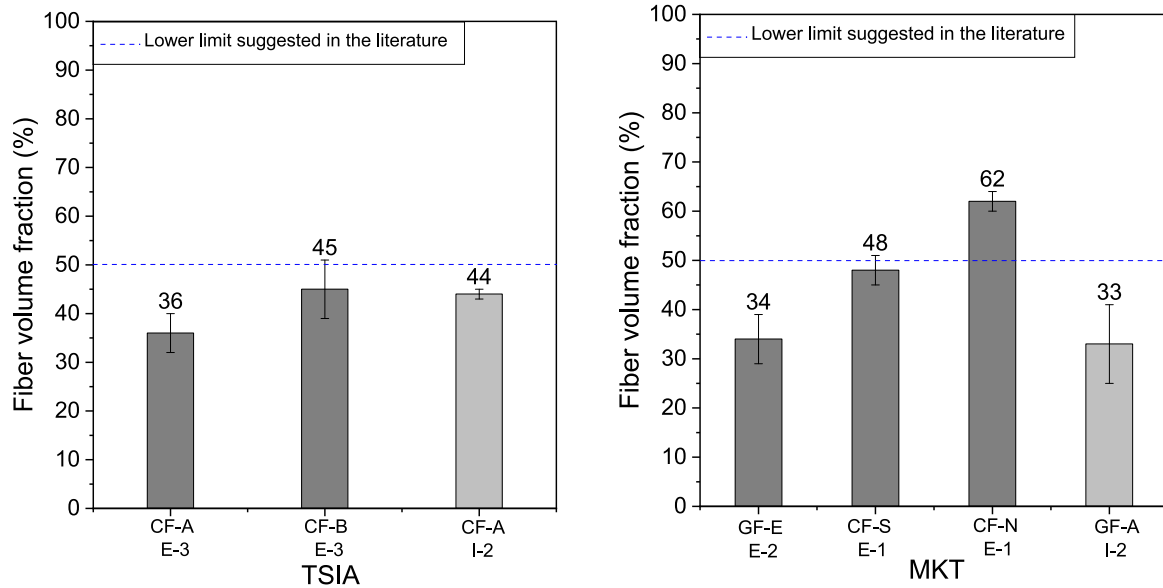


Fig. 16. Fiber volume content of TSIA and MKT retrofits determined by TGA.

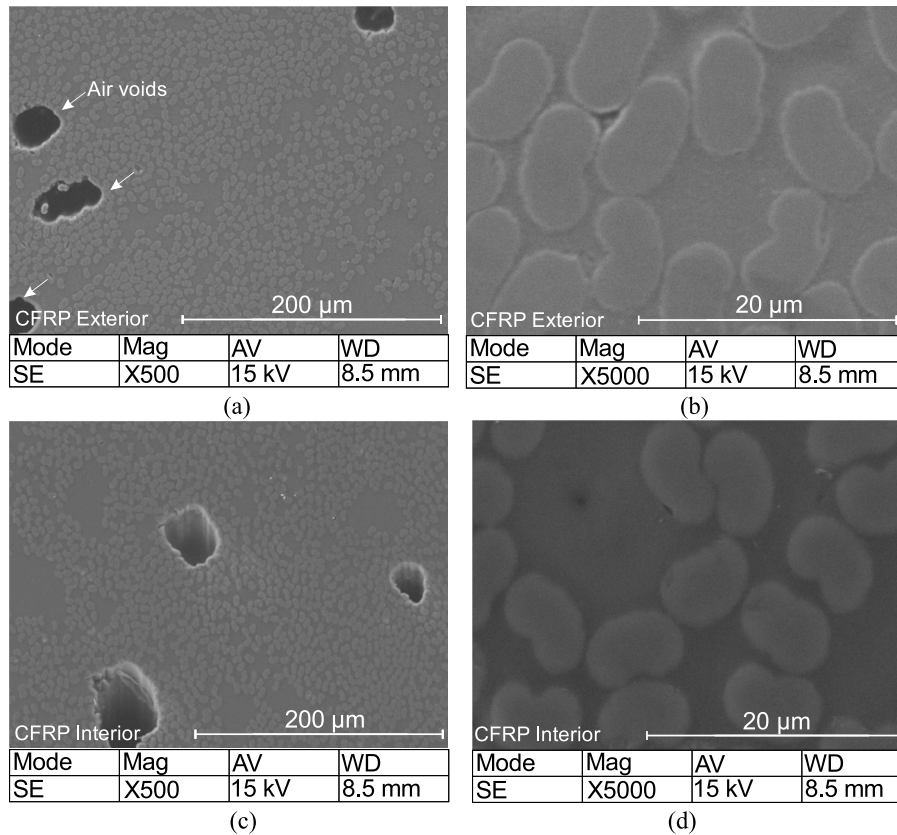


Fig. 17. SEM images of CFRP retrofits from TSIA: (a) Low magnification image of exterior CFRP retrofit, (b) high magnification image of exterior CFRP retrofit, (c) low magnification image of interior CFRP retrofit, and (d) high magnification image of interior CFRP retrofit.

relative weakness. Even small values of chemical shrinkage during the curing process can cause matrix failure at the fiber interface when fibers are closely-spaced [104]. There are a few other possible explanations for observed interfacial disruption of CFRP: mismatch in thermal coefficient between the fibers and matrix in combination with poor saturation (as this was not observed for CFRP at TSIA) [105,106], incompatibility between the fiber sizing and the matrix [107], and water absorption [108]. Interfacial bonding quality affects composite mechanical

properties on a macroscopic level and governs its durability [108]. Regions with air voids originating from impregnation are especially susceptible to water absorption, which can induce damage at the fiber-resin interface [102]. Non-uniformity in fiber packing causes a redistribution of the stresses and concentrations in the regions of minimum fiber distance [109]. In the literature, significantly higher stresses were observed in composites with random fiber distribution compared to composites in which regular fiber distribution was assumed [109]. Even a small

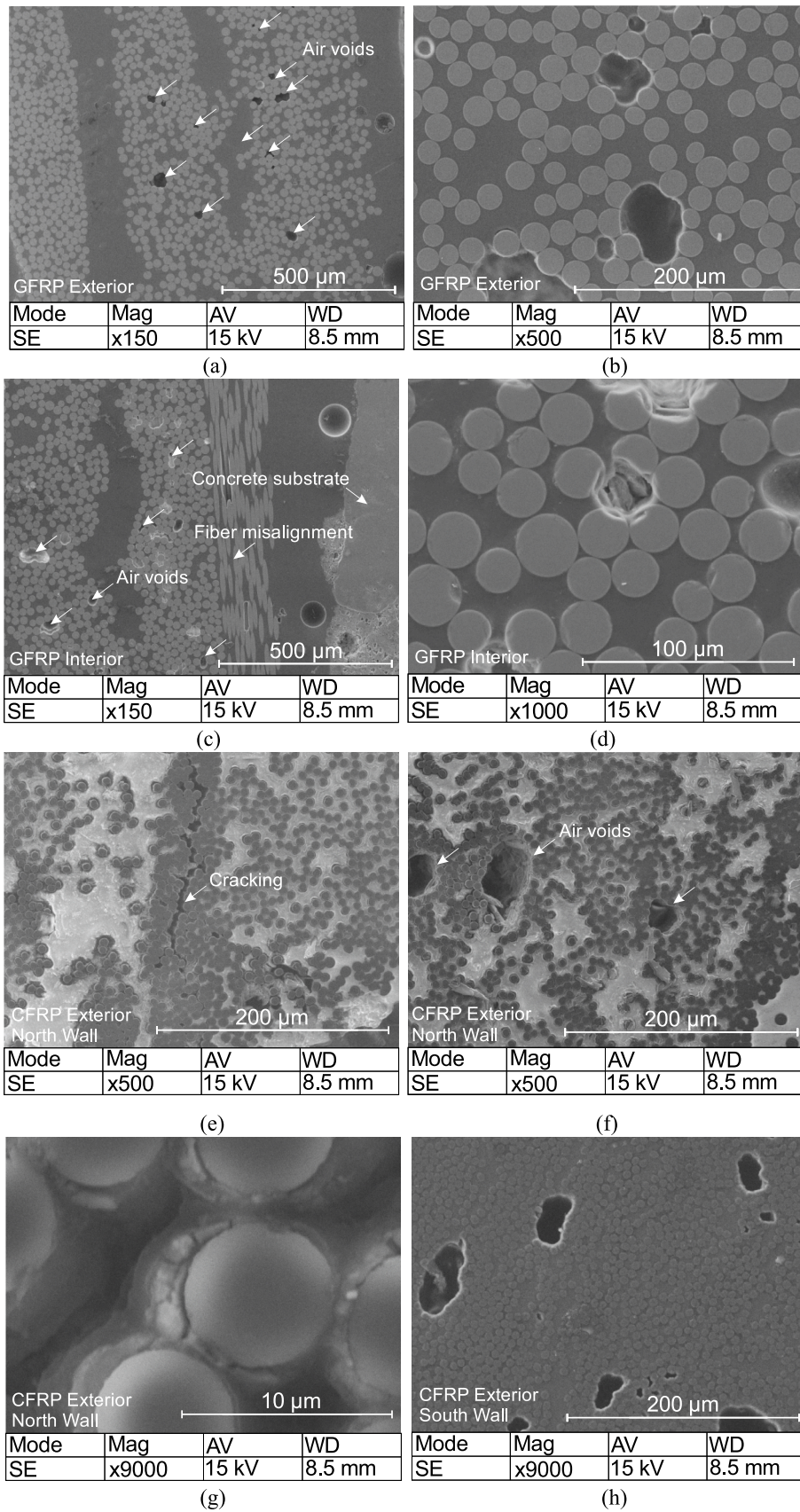


Fig. 18. SEM images of GFRP and CFRP retrofits from MKT: (a) Low magnification image of an exterior GFRP retrofit, (b) high magnification image of an exterior GFRP retrofit, (c) low magnification image of an interior GFRP retrofit, (d) high magnification image of an interior GFRP retrofit, (e) low magnification image of an exterior CFRP retrofit on the north wall, (f) low magnification image of an exterior CFRP retrofit on the north wall, (g) high magnification image of an exterior CFRP retrofit on the north wall, and (h) low magnification image of an exterior CFRP retrofit on the south wall.

misalignment of fibers has been shown to affect key mechanical properties—it may result in a decrease of tensile strength by as much as 13 % [110].

4. Summary and conclusions

The effect of long-term subarctic field exposure on the physical and chemical properties of FRP composites was evaluated by comparing exterior and interior FRP retrofits installed on two buildings located in Anchorage, AK. FRP composite retrofits installed on McKinley Tower and Ted Stevens International Airport, in 2004 and 2008, respectively, were analyzed using DSC, TGA, ATR-FTIR spectroscopy, Raman spectroscopy, and cross-sectional SEM imaging. Based on the experimental results, the following conclusions can be drawn:

- At TSIA, most exterior samples had significantly higher T_g values than the maximum T_g values measured on interior samples. An exception to this is one exterior sample with a T_g value 5 °C below the maximum interior temperature. Comparison with T_g values recommended in ACI 440.2R showed that the minimum value was met for the interior, but not for the exterior retrofits. Large scatter in T_g values of 17 °C at TSIA is evidence of how unpredictable the curing process of epoxy can be on the same construction site. When the epoxy is used in FRP applications in civil engineering, considerable scatter of T_g values should be accounted for in the design to achieve the desired levels of safety and reliability of FRP retrofitted structures under the maximum service temperature.
- At MKT, the T_g value for most exterior and interior samples was approximately 55 °C, except for the CFRP samples collected on the exterior north wall, which had T_g values of 45 °C and 50 °C. Lower values measured on the north wall can be either caused by lower curing temperature during installation, issues with the mix ratio of the two-component epoxy, or plasticization caused by moisture uptake during mixing of epoxy. Interior T_g values were above the minimum recommended T_g value per ACI 440.2R. On the other hand, T_g values of the exterior retrofits did not satisfy the minimum recommendation from ACI 440.2R which can potentially impact the load-carrying capacity of the structure at maximum service temperatures.
- Raman spectroscopy, used to investigate if the degree of cure affected T_g , showed a moderate correlation between the 1252 cm^{-1} peak intensity (as an indicator of the degree of cure) in Raman spectra and T_g value. Statistical analysis, based on the *t*-test, suggests that variability in the data can be only partially attributed to the variability in the degree of cure.
- No notable differences were observed in the ATR-FTIR spectra recorded on the exterior and interior retrofits from TSIA. Peaks in the (1500–1730) cm^{-1} range, related to epoxy oxidation, were observed in some samples at MKT. Chemical degradation of epoxy could not be confirmed due to potential interference with the paint residue. Micro-FTIR analysis conducted on the cross-section near the FRP surface (about 100 μm from the exterior surface of the composite) did not detect chemical degradation and indicates that if any chemical degradation occurred, it was limited to the surface of the composite.
- Air voids and non-uniform distribution of fibers in the matrix were observed in cross-sectional SEM images of all FRP retrofits from both buildings. There were no signs of degradation observed in the FRP retrofit samples from TSIA. However, cracking was observed in the region with closely packed fibers in CFRP samples from MKT.
- Fiber volume content, measured by TGA, was below 50 % for all retrofits from TSIA and MKT except CFRP on the north wall from MKT. The values varied considerably on both buildings but more significantly at MKT. Precisely, a significantly higher fiber content (62 % on the north wall and 48 % on the south wall) was measured in the CFRP samples from MKT compared to GFRP (33 % for both

interior and exterior retrofits). Insufficient saturation of CFRP (fiber weight fraction measured by TGA was 71 %), observed on the north wall at MKT is a concern since the increased presence of voids and micropores due to the lack of resin allows for penetration of water and aggressive chemicals to enter from the environment.

- Issues with the bond of exterior CFRP retrofits were previously reported as a part of our field study of building retrofits in Alaska [52]. Comparison of pull-off strength data and debonding between the exterior and interior at TSIA and MKT suggested that the bond is vulnerable to Alaska's climate. Unlike the CFRP/concrete bond, CFRP and GFRP composite long-term durability does not seem to be significantly affected by the Anchorage, AK climate for the time frame and applications considered in this work. Variability in T_g observed at TSIA is most probably due to weather conditions at the time of installation. Crack observed under the SEM in the CFRP sample from the north wall at MKT is likely a result of poor fiber saturation.

5. Recommendations for future field work

When physicochemical properties of field FRP samples are to be evaluated, special care must be taken to keep specimens' physical and chemical properties unchanged before testing. During sample collection and preparation for thermal and spectroscopic analyses, the following challenges were encountered and solutions were utilized to overcome these challenges:

1) All composite retrofits from the two buildings were painted. If not cleaned thoroughly, paint can introduce artifacts in the DSC measurements, FTIR spectra, and TGA data. Light sanding of samples followed by compressed air blowing are recommended for FTIR spectroscopy. The use of solvents is discouraged as solvents can introduce contamination, plasticization, and chemical changes to the sample. Sample preparation for FTIR was especially challenging because paint sanding can disturb a potentially degraded surface. To avoid this, FTIR analysis on the cross-section using micro-FTIR is considered a more desirable approach. Issues with sample contamination were also encountered in the DSC experiments. Some measurements had to be repeated due to the presence of spurious peaks and multiple transitions in the DSC curves, likely originating from the paint residue. Regarding TGA analysis, paint residue led to underestimation of fiber content in the composite. It is, therefore, recommended to use a razor blade to extract material from the bulk areas of the FRP samples for DSC and TGA characterization.

2) Collection of externally bonded FRP samples is typically conducted using saws or similar power tools that can generate heat which, in turn, can stimulate additional curing of the epoxy matrix. As a result, measured T_g values of the composite sample could be greater than its in-situ value. Extraction of samples should be conducted by using slow-speed diamond saws.

3) The hygric state of the samples in-situ and at the time of testing may be different, which can influence the T_g values. Specifically, water acts as a plasticizer in epoxy; if the sample dries over time, the T_g will increase as the plasticization process is semi-reversible. This is important if the decrease of T_g due to higher water content is to be captured. To keep the moisture content unchanged by the time samples are tested, sealed plastic bags are recommended for sample storing instead of paper bags. Samples should also not be transported and stored under elevated temperatures.

4) Portable moisture content measurements (near IR, for example) in-situ at the surface and at the FRP/concrete interface when removing samples might be helpful when collecting samples for DSC analysis.

5) The building owner should store FRP witness panels under ambient conditions to serve as a reference for evaluating long-term effects of environmental conditions on the physical, chemical properties, and microstructure of aged FRP composite materials. Historical tensile test data should also be maintained and accessible.

Disclaimer

Certain commercial products or equipment are described in this paper to adequately specify the experimental procedure. In no case does such identification imply recommendation or endorsement by the National Institute of Standards and Technology, nor does it imply that it is necessarily the best available for the purpose.

CRedit authorship contribution statement

Sandra Milev: Methodology, Formal analysis, Investigation, Writing – original draft, Writing – review & editing, Visualization, Data curation. **David Goodwin:** Conceptualization, Methodology, Investigation, Writing – original draft, Writing – review & editing, Supervision, Project administration. **Siamak Sattar:** Writing – review & editing, Supervision, Project administration. **Jovan Tatar:** Conceptualization, Methodology, Investigation, Writing – original draft, Writing – review & editing, Supervision, Project administration, Funding acquisition.

Declaration of Competing Interest

The authors declare that they have no known competing financial interests or personal relationships that could have appeared to influence the work reported in this paper.

Acknowledgement

Tatar gratefully acknowledges the financial support provided by the National Science Foundation to the University of Delaware under award number 1916972. Any opinions, findings, and conclusions or recommendations expressed in this paper are those of the authors and do not necessarily reflect the views of the National Science Foundation or National Institute of Standards and Technology. The authors would like to thank Quakewrap Inc. and Jeff Robertson, PE from Quakewrap Inc. for their assistance. Authors also thank staff at MKT and TSIA for providing access to field sites and assistance with sample collection.

References

- [1] S. Nolan, M. Rossini, C. Knight, A. Nanni, New directions for reinforced concrete coastal structures, *J Infrastruct Preserv Resil* 2 (2021) 1–12.
- [2] H.R. Hamilton, J. Brown, J. Tatar, M. Lisek, N.R. Brenkus, Durability evaluation of Florida's fiber-reinforced polymer (FRP) composite reinforcement for concrete structures. Research Report BDV31-977-01, Florida Department of Transportation, Gainesville, FL, USA. (2017).
- [3] J. Tatar, N.R. Brenkus, Performance of FRP-Strengthened Reinforced Concrete Bridge Girders after 12 Years of Service in Coastal Florida, *J Compos Constr* 25 (4) (2021), [https://doi.org/10.1061/\(ASCE\)CC.1943-5614.0001134](https://doi.org/10.1061/(ASCE)CC.1943-5614.0001134).
- [4] J. Tatar, D. Wagner, H.R. Hamilton, Structural Testing and Dissection of Carbon Fiber-Reinforced Polymer-Repaired Bridge Girders Taken Out of Service, *ACI Struct J* 113 (6) (2016).
- [5] E.P. Douglas, H.R. Hamilton III, J. Nino, Highly accelerated lifetime for externally applied bond critical fiber-reinforced polymer (FRP) infrastructure materials. Florida Department of Transportation, Research Report BDK75-977-45 (2014).
- [6] C.E. Bakis, L.C. Bank, V.L. Brown, E. Cosenza, J.F. Davalos, J.J. Lesko, A. Machida, S.H. Rizkalla, T.C. Triantafyllou, Fiber-reinforced polymer composites for construction - State-of-the-art review, *J Compos Constr* 6 (2) (2002) 73–87.
- [7] C.K. Ma, N.M. Apandi, S.C.S. Yung, N.J. Hau, L. Haur, A.Z. Awang, et al., Repair and rehabilitation of concrete structures using confinement : A review, *Constr Build Mater* 133 (2016) 502–515.
- [8] S. Marouani, L. Curtil, P. Hamelin, Instability of the performances of FRP composites implemented in civil engineering environment: Experimental study and durability implications, *Polym Polym Compos* 20 (2010) 387–398.
- [9] M. Al Azawani, P. Hopkins, G. Mullins, R. Sen, FRP-Concrete Bond after 12-Year Exposure in Tidal Waters, *J Compos Constr* 22 (2018) 1–15.
- [10] S. Marouani, L. Curtil, P. Hamelin, Composites realized by hand lay-up process in a civil engineering environment: Initial properties and durability, *Mater Struct Constr* 41 (5) (2008) 831–851.
- [11] R.J.C. Carbas, E.A.S. Marques, L.F.M. da Silva, A.M. Lopes, Effect of cure temperature on the glass transition temperature and mechanical properties of epoxy adhesives, *J Adhes* 90 (1) (2014) 104–119.
- [12] C.-S. Chern, G.W. Poehlein, A kinetic model for curing reactions of epoxides with amines, *Polym Eng Sci* 27 (11) (1987) 788–795.
- [13] H. Yamasaki, S. Morita, Two-step curing reaction of epoxy resin studied by thermal analysis and infrared spectroscopy, *Appl Spectrosc* 66 (8) (2012) 926–933.
- [14] G. Wisanrakkit, J.K. Gillham, The glass transition temperature (T_g) as an index of chemical conversion for a high-T_g amine/epoxy system: Chemical and diffusion-controlled reaction kinetics, *J Appl Polym Sci* 41 (1990) 2885–2929.
- [15] M. Michel, E. Ferrier, Effect of curing temperature conditions on glass transition temperature values of epoxy polymer used for wet lay-up applications, *Constr Build Mater* 231 (2020) 117206.
- [16] B.-G. Min, Z.H. Stachurski, J.H. Hodgkin, Cure kinetics of elementary reactions of a DGEBA/DDS epoxy resin: 1. Glass transition temperature versus conversion. *Polymer (Guildf)* 34 (23) (1993) 4908–4912.
- [17] J. Galy, A. Sabra, J.-P. Pascault, Characterization of epoxy Thermosetting Systems by Differential Scanning Calorimetry, *Polym Eng Sci* 26 (21) (1986) 1514–1523.
- [18] G.R. Palmese, R.L. McCullough, Effect of Epoxy-Amine Stoichiometry on Cured Resin Material Properties, *J Appl Polym Sci* 46 (1992) 1863–1873.
- [19] Y. Calventus, S. Montserrat, J.M. Hutchinson, Enthalpy relaxation of non-stoichiometric epoxy-amine resins, *Polymer (Guildf)* 42 (16) (2001) 7081–7093.
- [20] ACI 440.2R. Guide for the Design and Construction of Externally Bonded FRP Systems for Strengthening Concrete Structures. Am Concr Institute, Farming Hills, MI 48331 2017.
- [21] M. Lettieri, M. Frigione, Natural and Artificial Weathering Effects on Cold-Cured Epoxy Resins, *J Appl Polym Sci* 119 (3) (2011) 1635–1645.
- [22] ACI-440.2R. Guide for the Design and Construction of Externally Bonded FRP Systems for Strengthening Concrete Structures. Am Concr Inst Comm 440, Farming Hills, MI, USA 2017.
- [23] J. Tatar, S. Milev, Durability of externally bonded fiber-reinforced polymer composites in concrete structures: A critical review, *Polymers* 13 (5) (2021), <https://doi.org/10.3390/polym13050765>.
- [24] B.P. Blackburn, J. Tatar, E.P. Douglas, H.R. Hamilton, Effects of hygrothermal conditioning on epoxy adhesives used in FRP composites, *Constr Build Mater* 96 (2015) 679–689.
- [25] H. Maljaee, B. Ghiassi, P.B. Lourenço, Effect of synergistic environmental conditions on thermal properties of a cold curing epoxy resin, *Compos Part B Eng* 113 (2017) 152–163.
- [26] J. Shrestha, T. Ueda, D. Zhang, Durability of FRP Concrete Bonds and Its Constituent Properties under the Influence of Moisture Conditions, *J Mater Civ Eng* 27 (2015) 1–14.
- [27] J. Tatar, Nanomechanical properties of cement Paste-Epoxy interphase following hygrothermal conditioning by water immersion, *Constr Build Mater* 282 (2021), <https://doi.org/10.1016/j.conbuildmat.2021.122695>.
- [28] F.X. Perrin, M.H. Nguyen, J.L. Vernet, Water transport in epoxy-aliphatic amine networks - Influence of curing cycles, *Eur Polym J* 45 (5) (2009) 1524–1534.
- [29] M. Robert, P. Cousin, B. Benmokrane, Behaviour of GFRP reinforcing bars subjected to extreme temperatures, *Proceedings, Annu Conf - Can Soc Civ Eng* 3 (2009) 1587–1596.
- [30] F. Fraga, C. Castro-Diaz, E. Rodríguez-Núñez, J.M. Martínez-Ageitos, Physical aging for an epoxy network diglycidyl ether of bisphenol A/m-xylolenediamine, *Polymer (Guildf)* 44 (19) (2003) 5779–5784.
- [31] J.M. Hutchinson, Physical Aging of Polymers, *Prog Polym Sci* 20 (4) (1995) 703–760.
- [32] G.M. Odegard, A. Bandyopadhyay, Physical aging of epoxy polymers and their composites, *J Polym Sci Part B Polym Phys* 49 (24) (2011) 1695–1716.
- [33] W. Tian, J. Hodgkin, Long-term aging in a commercial aerospace composite sample: Chemical and physical changes, *J Appl Polym Sci* 115 (5) (2010) 2981–2985.
- [34] L. Belec, T.H. Nguyen, D.L. Nguyen, J.F. Chailan, Comparative effects of humid tropical weathering and artificial ageing on a model composite properties from nano- to macro-scale, *Compos Part A Appl Sci Manuf* 68 (2015) 235–241.
- [35] B. Mailhot, S. Morlat-Thérias, M. Ouahioune, J.-L. Gardette, Study of the degradation of an epoxy/amine resin, 1 photo- and thermo-chemical mechanisms. *Macromol, Chem Phys* 206 (5) (2005) 575–584.
- [36] S. Morsch, Y. Liu, S.B. Lyon, S.R. Gibbon, B. Gabriele, M. Malinin, K.-J. Eichhorn, Examining the early stages of thermal oxidative degradation in epoxy-amine resins, *Polym Degrad Stab* 176 (2020), 109147.
- [37] J.W. Chin, T. Nguyen, K. Aouadi, Sorption and Diffusion of Water, Salt Water, and Concrete Pore Solution in Composite Matrices, *J Appl Polym Sci* 71 (3) (1999) 483–492.
- [38] C. Bockenheimer, D. Fata, W. Possart, New aspects of aging in epoxy networks. II. Hydrothermal aging, *J Appl Polym Sci* 91 (1) (2004) 369–377.
- [39] Y.-C. Lin, X.-u. Chen, H.-J. Zhang, Z.-P. Wang, Effects of hygrothermal aging on epoxy-based anisotropic conductive film, *Mater Lett* 60 (24) (2006) 2958–2963.
- [40] Y.-M. Pei, K. Wang, M.-S. Zhan, W. Xu, X.-J. Ding, Thermal-oxidative aging of DGEBA/EPN/LMPA epoxy system: Chemical structure and thermal-mechanical properties, *Polym Degrad Stab* 96 (7) (2011) 1179–1186.
- [41] A. Rivaton, L. Moreau, J.-L. Gardette, Photo-oxidation of phenoxy resins at long and short wavelengths - I. Identification of the photoproducts, *Polym Degrad Stab* 58 (3) (1997) 321–332.
- [42] L. Monney, R. Belali, J. Vebrel, C. Dubois, A. Chambaudet, Photochemical degradation study of an epoxy material by IR-ATR spectroscopy, *Polym Degrad Stab* 62 (2) (1998) 353–359.
- [43] E. Ernault, E. Richaud, B. Fayolle, Thermal-oxidation of epoxy/amine followed by glass transition temperature changes, *Polym Degrad Stab* 138 (2017) 82–90, <https://doi.org/10.1016/j.polymdegradstab.2017.02.013>.
- [44] Y. Li, Atomistic Modeling of Environmental Aging of Epoxy Resins, Georgia Institute of Technology (2012).

- [45] H. Kaczmarek, Changes of polymer morphology caused by u.v. irradiation: 2. Surface destruction of polymer blends, *Polymer (Guildf)* 37 (4) (1996) 547–553.
- [46] V.M. Karbhari, Durability Gap Analysis for Fiber-Reinforced Polymer Composites in Civil Infrastructure, *J Compos Constr* 7 (2003) 219–237, [https://doi.org/10.1061/\(ASCE\)1090-0268\(2003\)7](https://doi.org/10.1061/(ASCE)1090-0268(2003)7).
- [47] A. Afshar, D. Mihut, J. Baqersad, S. Hill, Study of metallic thin films on epoxy matrix as protective barrier to ultraviolet radiation, *Surf Coatings Technol* 367 (2019) 41–48.
- [48] Goodwin DG, Sattar S, Dukes JD, Kim JH, Sung LP, Ferraris CC. Research Needs Concerning the Performance of Fiber Reinforced (FR) Composites Retrofit Systems for Buildings and Infrastructure. Spec Publ (NIST SP) - 1244 2019.
- [49] J. Tatar, C.R. Taylor, H.R. Hamilton, A multiscale micromechanical model of adhesive interphase between cement paste and epoxy supported by nanomechanical evidence, *Composit Part B: Eng* 172 (2019) 679–689, <https://doi.org/10.1016/j.compositesb.2019.05.038>.
- [50] J. Tatar, H.R. Hamilton, Implementation of bond durability in the design of flexural members with externally bonded FRP, *J Compos Constr* 20 (3) (2016), [https://doi.org/10.1061/\(ASCE\)CC.1943-5614.0000636](https://doi.org/10.1061/(ASCE)CC.1943-5614.0000636).
- [51] M.F. Green, L.A. Bisby, Y. Beaudoin, P. Labossière, Effect of freeze-thaw cycles on the bond durability between fibre reinforced polymer plate reinforcement and concrete, *Can J Civ Eng* 27 (5) (2000) 949–959.
- [52] J. Tatar, S. Sattar, D. Goodwin, S. Milev, S. Ahmed, J. Dukes, C. Segura, Performance of Externally Bonded Fiber Reinforced Polymer Retrofits in the 2018 Cook Inlet Earthquake in Anchorage, *Earthquake Spectra* 37 (4) (2021) 2342–2371.
- [53] F. Al-Mahmoud, J.M. Mechling, M. Shaban, Bond strength of different strengthening systems - Concrete elements under freeze-thaw cycles and salt water immersion exposure, *Constr Build Mater* 70 (2014) 399–409.
- [54] V.M. Karbhari, J. Rivera, J. Zhang, Low-temperature hygrothermal degradation of ambient cured E-glass/vinylester composites, *J Appl Polym Sci* 86 (9) (2002) 2255–2260.
- [55] V.M. Karbhari, M. Engineer, Effect of Environmental Exposure on the External Strengthening of Concrete with Composites-Short Term Bond Durability, *J Reinf Plast Compos* 15 (12) (1996) 1194–1216.
- [56] Y. Pan, D. Ph, G. Xian, H. Li, Effects of Freeze-Thaw Cycles on the Behavior of the Bond between CFRP Plates and Concrete Substrates, *J Compos Constr* 22 (2018) 1–14.
- [57] M. Frigione, A. Rodríguez-Prieto, Can accelerated aging procedures predict the long term behavior of polymers exposed to different environments, *Polymers (Basel)* 13 (16) (2021) 2688.
- [58] O. Moussa, A.P. Vassilopoulos, T. Keller, Effects of low-temperature curing on physical behavior of cold-curing epoxy adhesives in bridge construction, *Int J Adhes Adhes* 32 (2012) 15–22.
- [59] G.L.Martin. A New Life for an Old Building. *Alaska Bus Mon* 2005:37.
- [60] National Weather Service (2020). <https://www.nws.noaa.gov/climate.php/xmacis.php%3Fwfo=paic>.
- [61] S. Ebnesaajja, Surface and Material Characterization Techniques, *Surf. Treat. Mater. Adhes. Bond.* (2014).
- [62] S. Gao, Y.P. Koh, S.L. Simon, Calorimetric Glass Transition of Single Polystyrene Ultrathin Films, *Macromolecules* 46 (2) (2013) 562–570.
- [63] Astm e1356., Standard Test Method for Assignment of the Glass Transition Temperatures by Differential Scanning Calorimetry, *ASTM Int West Conshohocken, PA* (2008).
- [64] C.-R. Moon, B.-R. Bang, W.-J. Choi, G.-H. Kang, S.-Y. Park, A technique for determining fiber content in FRP by thermogravimetric analyzer, *Polym Test* 24 (3) (2005) 376–380.
- [65] R.Y. Yee, T.S. Stephens, A TGA technique for determining graphite fiber content in epoxy composites, *Thermochim Acta* 272 (1996) 191–199.
- [66] H. Vaskova, V. Kresálek, Quasi real-time monitoring of epoxy resin crosslinking via Raman microscopy, *Int J Math Model Methods Appl Sci* 5 (2011) 1197–1204.
- [67] TA Instruments. Characterization of Epoxy Reinforced Glass by DCS and DMA n. d.
- [68] M. Paroli, J.J. Penn, Measuring the glass-transition temperature of EPDM roofing materials: comparison of DMA, TMA and DSC techniques, *NRC Publ Arch NRCC-38551* (1995).
- [69] J. Michels, R. Widmann, C. Czaderski, R. Allahviridzadeh, M. Motavalli, Glass transition evaluation of commercially available epoxy resins used for civil engineering applications, *Compos Part B Eng* 77 (2015) 484–493.
- [70] AASHTO. AASHTO LRFDF Bridge Design Specifications. Am Assoc State Highw Transp Off Washington, DC 2017.
- [71] Bulletin-FIB-14. Externally bonded FRP reinforcement for RC structures 2001.
- [72] M. Jensen, J. Jakobsen, Effect of cure cycle on enthalpy relaxation and post shrinkage in neat epoxy and epoxy composites, *J Non Cryst Solids* 452 (2016) 109–113, <https://doi.org/10.1016/j.jnoncrysol.2016.08.032>.
- [73] C.J. deBakker, G.A. George, N.A. St John, P.M. Fredericks, The kinetics of the cure of an advanced epoxy resin by Fourier transform Raman and near-IR spectroscopy, *Spectrochim Acta Part A Mol Spectrosc* 49 (5-6) (1993) 739–752.
- [74] J. Rocks, L. Rintoul, F. Vohwinkel, G. George, The kinetics and mechanism of cure of an amino-glycidyl epoxy resin by a co-anhydride as studied by FT-Raman spectroscopy, *Polymer (Guildf)* 45 (20) (2004) 6799–6811.
- [75] M. Younes, S. Wartewig, D. Lellinger, B. Strehmel, V. Strehmel, The curing of epoxy resins as studied by various methods, *Polymer (Guildf)* 35 (24) (1994) 5269–5278.
- [76] J.W. Cooley, J.W. Tukey, An algorithm for the machine calculation of complex Fourier series, *Math Comput* 19 (90) (1965) 297–301.
- [77] A. Hale, C. Macosko, H. Bair, Glass Transition Temperature Function of Conversion in Thermosetting Polymers, *Macromolecules* 24 (1991) 2610–2621.
- [78] T.E. Twardowski, P.H. Geil, The effect of Chain Stiffness in Lightly Crosslinked Epoxies, *J Macromol Sci Part A* 30 (1) (1993) 75–89.
- [79] F. Meyer, G. Sanz, A. Eceiza, I. Mondragon, J. Mijović, The effect of stoichiometry and thermal history during cure on structure and properties of epoxy networks, *Polymer (Guildf)* 36 (7) (1995) 1407–1414.
- [80] A.F. Abdelkader, J.R. White, Water absorption in epoxy resins: The effects of the crosslinking agent and curing temperature, *J Appl Polym Sci* 98 (2005) 2544–2549, <https://doi.org/10.1002/app.22400>.
- [81] H. Kim, M.W. Urban, Molecular level chain scission mechanisms of epoxy and urethane polymeric films exposed to UV/H₂O, *Multidimensional spectroscopic studies. Langmuir* 16 (12) (2000) 5382–5390.
- [82] X. Reziq, T. Nguyen, D. Martin, L. Sung, X. Gu, J. Jasmin, J.W. Martin, Relationship between chemical degradation and thickness loss of an amine-cured epoxy coating exposed to different UV environments, *J Coatings Technol Res* 3 (3) (2006) 173–184.
- [83] F. Delor-Jestin, D. Drouin, P.-Y. Cheval, J. Lacoste, Thermal and photochemical ageing of epoxy resin - Influence of curing agents, *Polym Degrad Stab* 91 (6) (2006) 1247–1255.
- [84] A. Meiser, W. Possart, Epoxy-metal interphases: Chemical and mechanical aging, *J Adhes* 87 (4) (2011) 313–330.
- [85] X. Gu, T. Nguyen, M. Oudina, D. Martin, B. Kidah, J. Jasmin, A. Reziq, L. Sung, E. Byrd, J.W. Martin, D.L. Ho, Y.C. Jean, Microstructure and morphology of amine-cured epoxy coatings before and after outdoor exposures - An AFM study, *J Coatings Technol Res* 2 (7) (2005) 547–556.
- [86] M.G. González, J.C. Cabanelas, J. Baselga, Applications of FTIR on Epoxy Resins - Identification, Monitoring the Curing Process, Phase Separation and Water Uptake. *Infrared Spectrosc - Mater Sci, Eng Technol* 2 (2012).
- [87] Z. Wang, X.L. Zhao, G. Xian, G. Wu, R.K. Singh Raman, S. Al-Saadi, Durability study on interlaminar shear behaviour of basalt-, glass- and carbon-fibre reinforced polymer (B/G/CFRP) bars in seawater sea sand concrete environment, *Constr Build Mater* 156 (2017) 985–1004.
- [88] A.G. Xyla, P.G. Koutsoukos, Quantitative analysis of calcium carbonate polymorphs by infrared spectroscopy, *J Chem Soc Faraday Trans 1* (85) (1989) 3165–3172.
- [89] K.E. Chike, M.L. Myrick, R.E. Lyon, S.M. Angel, Raman and near-infrared studies of an epoxy resin, *Appl Spectrosc* 47 (10) (1993) 1631–1635.
- [90] B. Mailhot, S. Morlat-Thérias, P.-O. Bussière, J.-L. Gardette, Study of the degradation of an epoxy/amine resin, 2 kinetics and depth-profiles. *Macromol, Chem Phys* 206 (5) (2005) 585–591.
- [91] D.M. Hepburn, I.J. Kemp, J.M. Cooper, Degradation of filled epoxy resin surfaces, *Polym Degrad Stab* 70 (2) (2000) 245–251.
- [92] G.Z. Xiao, M.E.R. Shanahan, Irreversible effects of hygrothermal aging on DGEBA/DDA epoxy resin, *J Appl Polym Sci* 69 (2) (1998) 363–369.
- [93] J.C. Cabanelas, C. Antonelli, V.S. Miguel, J. Baselga, Spectroscopic Analysis of Epoxy/Thermoplastic Blends, *Handb Epoxy Blends* (2015) 1–30.
- [94] Dobbies A, Boll B, Fiedler B. Prediction of thermal exposure and mechanical behavior of epoxy resin using artificial neural networks and Fourier transform infrared spectroscopy. *Polymers (Basel)* 2019;11.
- [95] N. Poisson, G. Lachenal, H. Sautereau, Near- and mid-infrared spectroscopy studies of an epoxy reactive system, *Vib Spectrosc* 12 (2) (1996) 237–247.
- [96] R.E. Lyon, K.E. Chike, S.M. Angel, In situ cure monitoring of epoxy resins using fiber-optic Raman spectroscopy, *J Appl Polym Sci* 53 (1994) 1805–1812.
- [97] R. Hardis, J.L.P. Jessop, F.E. Peters, M.R. Kessler, Cure kinetics characterization and monitoring of an epoxy resin using DSC, Raman spectroscopy, and DEA, *Compos Part A Appl Sci Manuf* 49 (2013) 100–108.
- [98] L.C. Bank, T.R. Gentry, B.P. Thompson, J.S. Russell, A model specification for FRP composites for civil engineering structures, *Constr Build Mater* 17 (6-7) (2003) 405–437.
- [99] LARCO Ciprian, PAHONIE Radu, EDU Ioana, The Effects of Fibre Volume Fraction on a Glass-Epoxy Composite Material, *Incas Bull* 7 (3) (2015) 113–119.
- [100] S. Marouani, L. Curtil, P. Hamelin, Ageing of carbon/epoxy and carbon/vinylester composites used in the reinforcement and/or the repair of civil engineering structures, *Compos Part B Eng* 43 (4) (2012) 2020–2030.
- [101] A. Hammami, N. Al-Ghuilani, Durability and environmental degradation of glass-vinylester composites, *Polym Compos* 25 (6) (2004) 609–616.
- [102] L. Bian, J. Xiao, J. Zeng, S. Xing, Effects of seawater immersion on water absorption and mechanical properties of GFRP composites, *J Compos Mater* 46 (25) (2012) 3151–3162.
- [103] Z. Xu, J. Li, X. Wu, Y. Huang, L.I. Chen, G. Zhang, Effect of kidney-type and circular cross sections on carbon fiber surface and composite interface, *Compos Part A Appl Sci Manuf* 39 (2) (2008) 301–307.

- [104] A.R. Maligno, N.A. Warrior, A.C. Long, Effects of inter-fibre spacing on damage evolution in unidirectional (UD) fibre-reinforced composites, *Eur J Mech* 28 (4) (2009) 768–776.
- [105] A. Anvari, Effect of Temperature on the Mechanical Properties of Carbon Composites, *Journal of Engineering* 2020 (2020) 1–16.
- [106] A. Ali, Crack growth as a function of temperature variation in carbon fiber/epoxy, *J Chem Eng Mater Sci* 8 (3) (2017) 17–30.
- [107] J.D.H. Hughes, The carbon fibre/epoxy interface-A review, *Compos Sci Technol* 41 (1) (1991) 13–45.
- [108] L.-h. Tam, A.o. Zhou, R. Zhang, C. Wu, Effect of hygrothermal environment on traction-separation behavior of carbon fiber/epoxy interface, *Constr Build Mater* 220 (2019) 728–738.
- [109] A.J. Fletcher, J.L. Oakeshott, Thermal residual microstress generation during the processing of unidirectional carbon fibre/epoxy resin composites: random fibre arrays, *Composites* 25 (8) (1994) 806–813.
- [110] F. Nardone, M. Di Ludovico, Y. De Caso, F.J. Basalo, A. Prota, A. Nanni, Tensile behavior of epoxy based FRP composites under extreme service conditions, *Compos Part B Eng* 43 (2012) 1468–1474.